BBA - Molecular Cell Research 1867 (2020) 118720

Contents lists available at ScienceDirect

BBA - Molecular Cell Research

journal homepage: www.elsevier.com/locate/bbamcr

Interferon-γ and high glucose-induced opening of Cx43 hemichannels causes endothelial cell dysfunction and damage

Juan C. Sáez[a,b], Susana Contreras-Duarte[a,c], Valeria C. Labra[d], Cristian A. Santibañez[d], Luis A. Mellado[d], Carla A. Inostroza[d], Tanhia F. Alvear[d], Mauricio A. Retamal[e,f], Victoria Velarde[a], Juan A. Orellana[d,*]

[a] Departamento de Fisiología, Pontificia Universidad Católica de Chile, Santiago de Chile, Chile
[b] Instituto de Neurociencias, Centro Interdisciplinario de Neurociencias de Valparaíso, Universidad de Valparaíso, Valparaíso, Chile
[c] Departamento de Ginecología y Obstetricia, Escuela de Medicina, Facultad de Medicina, Pontificia Universidad Católica de Chile, Santiago, Chile
[d] Departamento de Neurología, Escuela de Medicina and Centro Interdisciplinario de Neurociencias, Facultad de Medicina, Pontificia Universidad Católica de Chile, Santiago, Chile
[e] Universidad del Desarrollo, Centro de Fisiología Celular e Integrativa, Facultad de Medicina Clínica Alemana, Santiago, Chile
[f] Department of Cell Physiology and Molecular Biophysics, Center for Membrane Protein Research, Texas Tech University Health Sciences Center, Lubbock, TX, USA

ARTICLE INFO

Keywords:
Connexons
Hemichannels
Endothelium
Inflammation
Diabetes

ABSTRACT

Both IFN-γ or high glucose have been linked to systemic inflammatory imbalance with serious repercussions not only for endothelial function but also for the formation of the atherosclerotic plaque. Although the uncontrolled opening of connexin hemichannels underpins the progression of various diseases, whether they are implicated in endothelial cell dysfunction and damage evoked by IFN-γ plus high glucose remains to be fully elucidated. In this study, by using live cell imaging and biochemical approaches, we demonstrate that IFN-γ plus high glucose augment endothelial connexin43 hemichannel activity, resulting in the increase of ATP release, ATP-mediated Ca^{2+} dynamics and production of nitric oxide and superoxide anion, as well as impaired insulin-mediated uptake and intercellular diffusion of glucose and cell survival. Based on our results, we propose that connexin 43 hemichannel inhibition could serve as a new approach for tackling the activation of detrimental signaling resulting in endothelial cell dysfunction and death caused by inflammatory mediators during atherosclerosis secondary to diabetes mellitus.

1. Introduction

The endothelium promptly responds to acute damage producing and releasing a diversity of bioactive substances to control blood flow, vascular tone and permeability, blood coagulation and fibrinolysis processes, as well as redox balance and inflammatory responses [1]. However, during chronic challenges, endothelial cells become a source of inflammatory molecules that precipitate macrophage recruitment and dysfunctional angiogenesis with significant and potentially negative consequences for proper vascular homeostasis [2]. Relevantly, the incidence of atherosclerosis in diabetic patients is substantially higher in relation to the nondiabetic population [3] and the chronic activation of endothelial cells seems crucial in this phenomenon [4]. Although diverse factors underlie the progression of atherosclerosis in patients with Diabetes Mellitus (DM), one of the most crucial element is hyperglycemia associated to insulin resistance [5,6]. Hyperglycemia lead to systemic inflammatory imbalance with serious repercussions not only for endothelial function [4] but also for the formation of the atherosclerotic plaque [7].

Interferon-gamma (IFN-γ), a pleiotropic macrophage-stimulating cytokine secreted by T cells and natural killer cells, is considered a key factor involved in plaque destabilization [8,9]. IFN-γ enhances T helper type 1 cell immune response by upregulating class I and II antigens in the endothelium, vascular smooth muscle cells and monocyte–macrophages along with foam cells [10]. Despite that previous data have shown that IFN-γ operates on the endothelium by disturbing its morphology and barrier permeability [11,12]; the direct effect of this cytokine (not through leukocyte-mediated mechanisms) on other endothelial functions has been less studied. Moreover, although is expected that inflammation would act in synergy with hyperglycemia to induce endothelial malfunctioning and further atherosclerosis in diabetic patients with poor glycemic control, the interplay between high

* Corresponding author at: Laboratorio de Neurociencias, Escuela de Medicina, Pontificia Universidad Católica de Chile, Marcoleta 391, 8330024, Santiago, Chile.
E-mail address: jaorella@uc.cl (J.A. Orellana).

https://doi.org/10.1016/j.bbamcr.2020.118720
Received 21 January 2020; Received in revised form 9 April 2020; Accepted 12 April 2020
Available online 14 April 2020
0167-4889/ © 2020 Elsevier B.V. All rights reserved.

glucose and IFN-γ in this process has not been well elucidated. Recently, we demonstrated that high glucose in concomitance with interleukin-1β (IL-1β) and tumor necrosis factor-α (TNF-α) increases adenosine triphosphate (ATP)-dependent Ca^{2+} responses and nitric oxide (NO) generation in endothelial cells by a mechanism that involves the activation of hemichannels [13,14]. These channels are located in the plasma membrane and consist of six connexin subunits that oligomerize around a central pore, allowing the diffusion of ions and small molecules that underpin the autocrine/paracrine signaling and exchange between intra- and extracellular compartments [15]. During particular pathophysiological conditions, as opposed to being favorable, the persistent activity of hemichannels underpins detrimental processes by various mechanisms, such as the increased release of potentially toxic molecules, intracellular Ca^{2+} imbalance and ionic/osmotic disturbances [16]. A pivotal element behind this process is related to the increased release of inflammatory mediators as a result of the disturbed operation of the immunological response [17].

Despite that prior data have shown that IFN-γ plus TNF-α increase connexin hemichannel activity in cultured microglia [18], whether IFN-γ and/or high glucose can regulate hemichannel opening in the endothelium is still unknown. We speculate that high glucose along with IFN-γ enhance hemichannel opening in endothelial cells, triggering changes not only on cell function but also in cell survival. In this study, we demonstrated that high glucose concentration and IFN-γ augment the activity of endothelial connexin43 (Cx43) hemichannels. Moreover, IFN-γ in combination with high glucose raised the release of ATP and prostaglandin E_2 (PGE_2), ATP-mediated Ca^{2+} dynamics and production of NO and superoxide anion, but decreased insulin-mediated uptake and intercellular diffusion of glucose and cell survival. Notably, the blockade of Cx43 hemichannels prevents these events.

2. Materials and methods

2.1. Reagents and antibodies

HEPES, water (W3500), Dulbecco's Modified Eagle Medium (DMEM), sc-19,220, indometacin, L-N6, SB203580, Lucifer yellow (LY), A74003, MRS2179, La^{3+}, oxidized ATP (oATP), ns-398, Cx43 rabbit polyclonal antibody (SAB4501174), ethidium (Etd) bromide, and probenecid (Prob) were acquired from Sigma-Aldrich (St. Louis, MO, USA). Fetal bovine serum (FBS) was purchased from Hyclone (Logan, UT, USA). Penicillin, BAPTA-AM, goat anti-mouse Alexa Fluor 488, streptomycin, FURA-2 AM, MitoSOX™ Red, DAF-FM diacetate and diamidino-2-phenylindole (DAPI) were purchased from Thermo Fisher Scientific (Waltham, MA, USA). Normal goat serum (NGS) was purchased from Zymed (San Francisco, CA, USA). The anti-Cx43 mouse monoclonal antibody (610061) was obtained from BD Biosciences (Franklin Lakes, NJ, USA). IFN-γ was acquired from Roche Diagnostics (Indianapolis, MI, USA). The anti-α tubulin mouse monoclonal antibody (ab7291) and anti-α 1 Na^+/K^+ ATPase mouse monoclonal antibody (ab7671) were purchased from Abcam (Cambridge, UK). Horseradish peroxidase (HRP)-conjugated anti-rabbit IgG, Sulfo-NHS-SS-biotin, and NeutrAvidin immobilized on agarose beads were obtained from Pierce (Rockford, IL, USA). The mimetic peptides gap19 (KQIEIKKFK, intracellular loop domain of Cx43), Tat-L2 (YGRKKRRQRRRDGANVDMHLKQIEIKKFKYGIEEHGK, second intracellular loop domain of Cx43), gap27 (SRPTEKTIFFI, second extracellular loop domain of Cx43) and ^{10}panx1 (WRQAAFVDSY, first extracellular loop domain of Panx1) were obtained from Genscript (New Jersey, USA).

2.2. Cell cultures

The human endothelial cell line EAhy 926 was kindly donated by Cora-Jean S. Edgell, University of North Carolina, Chapel Hill. EAhy cells were seeded onto plastic dishes (Nunclon) or onto glass coverslips (Gassalem, Limeil-Brevannes, France) in DMEM, supplemented with penicillin (5 U/ml), streptomycin (5 μg/ml), and 10% FBS and kept at 37 °C in a 5% CO_2/95% air atmosphere at nearly 100% relative humidity. Passaging was performed at ~90% confluence and cells were re-seeded at 1×10^4 cells/cm^2.

2.3. Treatments

Cells were treated for 1, 24, 48 or 72 h with IFN-γ (2.5 ng/ml) in concomitance with different concentrations of glucose (5, 25 or 45 mM). To obtain conditioned media (CM) from cells, they were seeded (2×10^6 cells in 35 mm dishes) in DMEM containing 10% FBS and treated with 2.5 ng/ml IFN-γ for 72 h. Supernatants were collected, filtered (0.22 μm), and stored at −20 °C before used for experiments. Mimetic peptides against Cx43 hemichannels (100 μM gap19, gap27 or Tat-L2) and pannexin1 (Panx1) channels (100 μM ^{10}panx1), as well as La^{3+} (200 μM) and Prob (500 μM), were used in cell cultures 15 min prior to and co-applied with Etd for time-lapse recordings (see below). In sister experiments, SB203580 (p38 mitogen-activated protein kinase (MAPK) inhibitor), L-N6 (inducible NO synthase [iNOS] inhibitor), indomethacin (cyclooxygenase-1 [COX_1] and cyclooxygenase-2 [COX_2] inhibitor), sc-560 (COX_1 inhibitor), ns-398 (COX_2 inhibitor), sc-19,220 (PEG_2 receptor 1 (EP_1) antagonist), BAPTA-AM (intracellular Ca^{2+} chelator), oATP ($P2X_7$ antagonist), MRS2179 ($P2Y_1$ antagonist) or A740003 ($P2X_7$ antagonist) were applied 1 h prior to and co-incubated with IFN-γ plus 25 mM glucose for 72 h or more.

2.4. siRNA transfection

siRNA duplexes against human Cx43 or Panx1 were predesigned and purchased from Origene (Rockville, MD). siRNA (10 nM) was transfected using Oligofectamine (Invitrogen) according to the Origene application guide for Trilencer-27 siRNA. Sequences for siRNAs against human Cx43 and Panx1 were: siRNA-Cx43: GCCTTCTTGCTGATCCAG TGGTACATC and siRNA-Panx1: GATCTCGATTGGTACACAGATAAG CTG, respectively. Transfection experiment were performed 24 h before treating cells with IFN-γ plus 25 mM glucose for 72 h.

2.5. Dye uptake and time-lapse fluorescence imaging

For time-lapse fluorescence imaging, cells plated on glass coverslips were washed twice in Hank's balanced salt solution. Then, cells were bathed in Locke's solution containing 5 μM Etd and mounted on the stage of an Olympus BX 51W1I upright microscope with a 40× water immersion objective for time-lapse imaging. Images were acquired using a Retiga 1300I fast-cooled monochromatic digital camera (12-bit) (Qimaging, Burnaby, BC, Canada) controlled by imaging software Metafluor software (Universal Imaging, Downingtown, PA) every 30 s (exposure time = 0.5 s; excitation and emission wavelengths were 528 nm 598 nm, respectively). The fluorescence intensity recorded from 25 regions of interest (representing 25 cells per field and coverslip) was defined as the subtraction (F−F0) between the fluorescence (F) from respective cell and the background fluorescence (F0) measured where no labeled cells were detected. The mean slope of the relationship F−F0 over a given time interval (ΔF/ΔT; F0 remained constant along the recording time) represents the Etd uptake rate. To measure the changes in slope, regression lines were fitted to points before and after the different experimental conditions using Excel software, and mean values of slopes were compared using GraphPad Prism software and expressed as AU/min. At least four replicates (four sister coverslips) were measured in each independent experiment.

2.6. Whole cell patch-clamp recordings

Cells at 60–70% confluence were detached with 1 ml of 0.25% trypsin–EDTA for 1–2 min at 37 °C, then placed in a 15 ml tube containing 3 ml D-MEM plus 10% FBS, centrifuged at 100 ×*g* for 2 min.

Supernatant was discharged and cells resuspended at 1×10^6 cells/ml in fresh extracellular recording media (in mM): 145 NaCl, 4 KCl, 1.8 $CaCl_2$, 1 $MgCl_2$, 10 HEPES, and 10 glucose, pH 7.4 (adjusted with NaOH). Following a recovery period (30 min at room temperature), cells were gently resuspended and 6 µl of cell suspension were placed in the Patchliner (NPC-16 Patchliner system, Nanion Technologies GmbH, Germany). Patch-control HT software (HEKA Elektronik, Germany) was used to control the pressure necessary to establish the whole-cell configuration. Hemichannel currents were recorded at room temperature (22–23 °C), using as internal solution (in mM): 10 NaF, 110 CsF, 20 CsCl, 2 EGTA, and 10 HEPES, pH 7.4 (adjusted with CsOH) and an external solution described above. Following cell contact with the 3–5 MΩ planar electrode, 6.6 µl of seal enhancer solution (in mM: 80 NaCl, 3 KCl, 35 $CaCl_2$, 10 HEPES/NaOH pH 7.4) were added to the external solution to promote giga-ohm seal formation. After establishing the whole-cell configuration, the seal enhancer solution was replaced with two washes of fresh external solution and the series resistance was compensated (50%, 10 µS). Cells were allowed to stabilize for 2 min after starting whole-cell recordings. Patchmaster software (HEKA) was used to automatically compensate whole-cell capacitance and series resistance, and perform voltage-clamp protocols.

2.7. Western blot analysis

Cells were bathed twice with PBS (pH 7.4) and harvested by scraping with a plastic scraper in ice-cold PBS containing 5 mM EDTA, Halt (78440) and M-PER protein extraction cocktail (78501) as stated in the manufacturer datasheet (Pierce, Rockford, IL, USA). The cell suspension was sonicated on ice and proteins were measured using the Bio-Rad Bradford assay. Aliquots of cell lysates (100 µg of protein) were resuspended in Laemmli's sample buffer, separated in an 8% sodium dodecyl sulfate polyacrylamide gel electrophoresis (SDS-PAGE) and electro-transferred to nitrocellulose sheets. Nonspecific protein binding was blocked by incubation of nitrocellulose sheets in PBS-BLOTTO (5% nonfat milk in PBS) for 30 min. Blots were then incubated with Cx43 rabbit polyclonal antibody at 4 °C overnight, followed by four 15 min washes with PBS. Afterwards, blots were incubated with HRP- conjugated goat anti-rabbit antibody at room temperature for 1 h and then rinsed four times with PBS for 15 min each period. Immunoreactivity was detected by enhanced chemiluminescence reaction using the SuperSignal kit (Pierce, Rockford, IL) according to the manufacturer's instructions.

2.8. Cell surface biotinylation and quantification

Cells cultured on 100-mm dishes were bathed three times with ice-cold Hank's saline solution (pH 8.0), and 3 ml of sulfo-NHS-SS-biotin solution (0.5 mg/ml) was added followed by a 30 min incubation at 4 °C. Then, cells were washed three times with ice-cold saline containing 15 mM glycine (pH 8.0) to block unreacted biotin. The cells were harvested and incubated with an excess of immobilized NeutrAvidin (1 ml of NeutrAvidin per 3 mg of biotinylated protein) for 1 h at 4 °C after which 1 ml of wash buffer (saline solution, pH 7.2 containing 0.1% SDS and 1% Nonidet P-40) was added. The mixture was centrifuged for 2 min at 600 ×*g*. at 4 °C. The supernatant was removed and discarded, and the pellet was resuspended in 40 µl of saline solution, pH 2.8 containing 0.1 M glycine, to release the proteins from the biotin. After the mixture was centrifuged at 600 ×*g* at 4 °C for 2 min, the supernatant was collected, and the pH was adjusted immediately by adding 10 µl of 1 M Tris, pH 7.5. Relative protein levels were measured using Western blot analysis as described above. Resulting immunoblot signals were scanned, and the densitometric analysis was performed with IMAGEJ software.

2.9. Scrape loading/dye transfer assay

The functional state of gap junctions was evaluated at room temperature using the scrape-loading/dye transfer (SL/DT) technique. Briefly, cell cultures were washed for 10 min in HEPES-buffered salt solution (containing the following in mM: 140 NaCl, 5.5 KCl, 1.8 $CaCl_2$, 1 $MgCl_2$, 5 glucose, 10 HEPES, pH 7.4) followed by washing in a Ca^{2+}-free HEPES solution for 1 min. Then, a razor blade cut was made in the monolayer in a HEPES-buffered salt solution with normal Ca^{2+} concentration containing the fluorescent dye Lucifer yellow (LY). After 1 min, LY (100 µM) was washed out several times with HEPES-buffered salt solution. At 8 min after scraping, fluorescent images were captured using an Olympus BX 51W1I upright microscope with a 40× water immersion objective. Changes were monitored using an imaging system equipped with a Retga 1300I fast-cooled monochromatic digital camera (12-bit) (Qimaging, Burnaby, BC, Canada), monochromator for fluorophore excitation, and Metafluor software (Universal Imaging, Downingtown, PA) for image acquisition and analysis. For each trial, data were quantified by measuring fluorescence areas in three representative fields. Quantification of changes in gap junctional communication induced by different treatments was performed by measuring the fluorescence area, expressed as arbitrary units (AU).

2.10. Immunofluorescence

Cells grown on glass coverslips were fixed at room temperature with 2% paraformaldehyde for 30 min and then washed three times with PBS. Then, cells were incubated three times for 5 min in 0.1 M PBS-glycine, followed by 30 min incubation with 0.1% Triton X-100 in PBS containing 10% NGS. The permeabilized cells were incubated anti-Cx43 monoclonal antibody (BD Biosciences, 1:400) diluted in 0.1% PBS-Triton X-100 with 2% NGS at 4 °C overnight. After five rinses in 0.1% PBS-Triton X-100, cells were incubated with goat anti-mouse IgG Alexa Fluor 488 (1:1000) or Alexa Fluor 555-phalloidin at room temperature for 50 min. After several rinses, coverslips were mounted in DAPI-Fluoromount-G medium and examined with an Olympus BX 51W1I upright microscope with a 40 X water immersion objective or a confocal laser-scanning microscope with a 63 X objective (Olympus, Fluoview FV1000, Tokyo, Japan).

2.11. Measurement of PGE_2

The concentration of PGE_2 was determined in the endothelial CM. Samples were centrifuged at 14.000 ×*g* for 40 min and supernatants were collected and protein content assayed by the BCA method. The concentration of PGE_2 was measured using an enzyme-linked immunosorbent assay (ELISA) kit (KHL1701), according to the manufacturer's protocol (Thermo Fisher Scientific, Waltham, MA, USA).

2.12. Intracellular Ca^{2+} and NO imaging

Cells plated on glass coverslips were loaded with 5 µM Fura-2-AM or 5 µM DAF-FM diacetate in DMEM without serum at 37 °C for 45 min and then washed three times in Locke's solution (154 mM NaCl, 5.4 mM KCl, 2.3 mM $CaCl_2$, 5 mM HEPES, pH 7.4) followed by de-esterification at 37 °C for 15 min. The experimental protocol for Ca^{2+} signal and nitric oxide (NO) imaging involved data acquisition every 5 s (emission at 510 and 515 nm, respectively) at 340/380-nm and 495 excitation wavelengths, respectively, using an Olympus BX 51W1I upright microscope with a 40× water immersion objective. Changes were monitored using an imaging system equipped with a Retga 1300I fast-cooled monochromatic digital camera (12-bit) (Qimaging, Burnaby, BC, Canada), monochromator for fluorophore excitation, and METAFLUOR software (Universal Imaging, Downingtown, PA) for image acquisition and analysis. Analysis involved determination of pixels assigned to each cell. The average pixel value allocated to each cell was obtained with

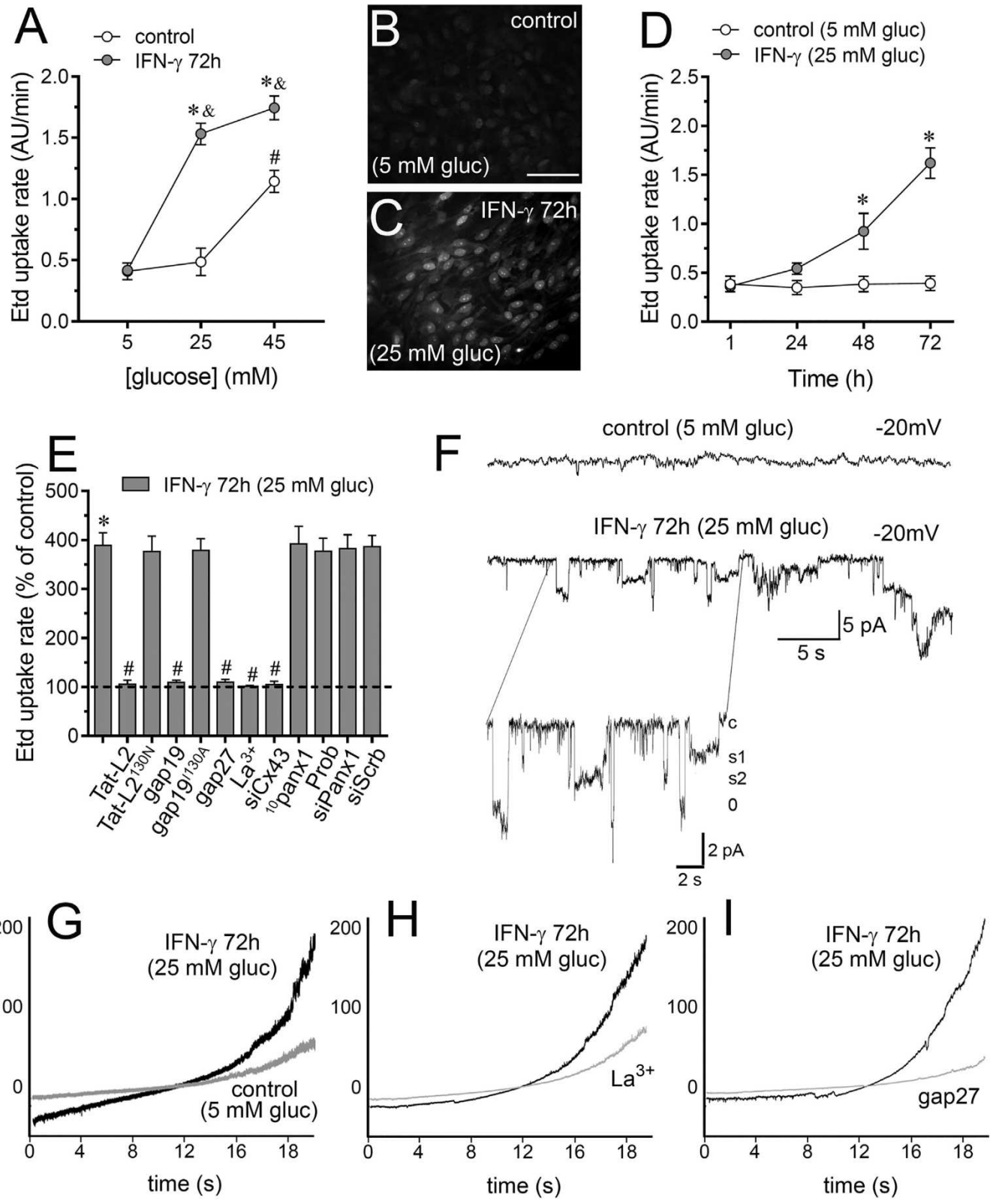

(caption on next page)

excitation at each wavelength and corrected for background. Due to the low excitation intensity, no bleaching was observed even when cells were illuminated for a few minutes. The FURA-2 ratio was obtained after dividing the 340-nm by the 380-nm fluorescence image on a pixel-by-pixel base ($R = F_{340\ nm}/F_{380\ nm}$).

2.13. Measurement of extracellular ATP concentration

Cells were seeded (2×10^6 cells in plastic tissue culture dishes of 35 mm in diameter) in DMEM containing 10% FBS and treated with IFN-γ plus 25 mM glucose for 72 h. Supernatants were collected, filtered

Fig. 1. IFN-γ plus high glucose increases the activity of Cx43 hemichannels in endothelial cells. (**A**) Averaged Etd uptake rate of EAhy cells treated for 72 h with different concentrations of glucose alone (control, white circles) or in combination with IFN-γ (blue circles; 2.5 ng/ml). $^{\#}p < .05$, 45 mM glucose (control) compared to 5 mM glucose (control), *p < .05, IFN-γ compared to control; $^{\&}p < .05$, high glucose (IFN-γ) compared to 5 mM glucose (IFN-γ) (two-way ANOVA followed by Tukey's post-hoc test). (**B**–**C**) Representative images Etd-nucleus (white) staining from dye uptake measurements (10 min exposure to dye) in EAhy cells treated for 72 h with 5 mM glucose (control, **B**) or 25 mM glucose and IFN-γ (**C**). (**D**) Averaged Etd uptake rate by EAhy cells treated for several time periods with 5 mM glucose (control, white circles) or 25 mM glucose and IFN-γ (blue circles). *p < .05, IFN-γ plus high glucose compared to control (two-way ANOVA followed by Tukey's post-hoc test). (**E**) Averaged Etd uptake rate normalized with control condition (dashed line) by EAhy cells treated for 72 h with 25 mM glucose and IFN-γ alone or in combination with the following blockers: 100 μM Tat-L2, 100 μM Tat-L2$^{H126K/I130N}$,100 μM gap19, 100 μM gap19 ^{I130A}, 100 μM gap27, 200 μM La^{3+}, siRNA^{Cx43}, 100 μM ^{10}panx1, 500 μM Probenecid (Prob), siRNA^{Panx1}; and siRNA^{scrb}. *p < .05, IFN-γ plus high glucose compared to control; $^{\#}p < .05$, effect of blockers compared IFN-γ plus high glucose (one-way ANOVA followed by Tukey's post-hoc test). Data were obtained from at least three independent experiments with four repeats each one (≥35 cells analyzed for each repeat). (**F**) Whole-cell voltage clamp recordings at −20 mV in EAhy cells treated for 72 h with 5 mM glucose (control, upper recording) or IFN-γ plus 25 mM glucose (below recording). Unitary current events from the below recording are also shown, where at least two sub conductance and one full open state were detected. (**G-I**) Voltage ramps from −80 to +80 mV in EAhy cells treated for 72 h with 5 mM glucose (control, gray line in **G**), IFN-γ plus 25 mM glucose (black line in **G**, **H**, and **I**) alone or in combination with 200 μM La^{3+} (gray line in **H**) or 100 μM gap27 (gray line in **I**). Calibration bar = 50 μm.

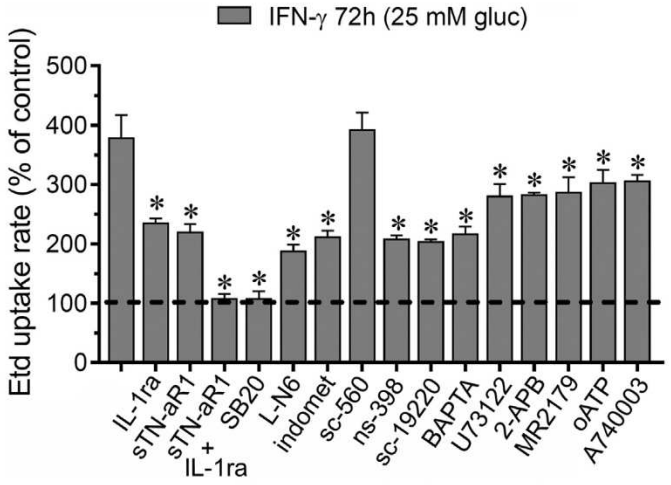

Fig. 2. Endothelial Cx43 hemichannel opening caused by and IFN-γ plus high glucose depends on Ca^{2+} signaling and activation of TNF-α/IL-1β/p38 MAPK/iNOS/COX_2/PLC-dependent pathways and EP_1/P2/IP_3 receptors. (**A**) Averaged Etd uptake rate normalized with control conditions (5 mM glucose, dashed line) of EAhy cells treated for 72 h with IFN-γ and 25 mM glucose alone or in combination with the following agents: 100 ng/mL of IL-1ra, 100 ng/mL of sTNF-αR1, 100 ng/mL of IL-1ra + 100 ng/mL of sTNF-αR1, 1 μM SB203580, 1 μM L-N6, 15 μM indometacin (indomet); 20 nM sc-560; 5 μM ns-398; 20 μM sc-19,220, 10 μM BAPTA, 5 μM U-73122, 50 μM 2-APB, 1 μM MRS2179, 200 μM oxidized ATP (oATP), and 200 nM A740003. *$p < .05$, effect of blockers compared to IFN-γ plus high glucose (one-way ANOVA followed by Tukey's post-hoc test). Data were obtained from at least three independent experiments with four repeats each one (≥35 cells analyzed for each repeat).

(0.22 μm), and stored at −20 °C before being used for experiments. Then, extracellular ATP was measured using a luciferin/luciferase bioluminescence assay kit (Sigma-Aldrich). The amount of ATP in each sample was inferred from standard curves and normalized for the protein concentration as determined by the BCA assay (Pierce).

2.14. 2-NBDG glucose uptake

Cells plated on glass coverslips were incubated with 500 μM 2-[N-(7-nitrobenz-2-oxa-1,3-diaxol-4-yl) amino]-2-deoxyglucose (2-NBDG) glucose analogue (342.3 g/mol, neutral, ThermoFisher, Carlsbad, CA) for 30 min at room temperature in Locke's solution (154 mM NaCl, 5.4 mM KCl, 2.3 mM $CaCl_2$, 5 mM HEPES, pH 7.4). Then, the cells were fixed with 4% PFA for 15 min at room temperature. Immunofluorescence pictures were captured at 495 excitation wavelength and the emission was filtered at 505–550 nm using an Olympus BX 51W1I upright microscope with a 40× water immersion objective. The average pixel value allocated to each cell was measured with Metafluor software (Universal Imaging, Downingtown, PA) and corrected for background.

2.15. Intercellular 2-NBDG glucose diffusion

Cells plated on glass coverslips were bathed with a recording medium (HCO_3^--free F-12 medium buffered with 10 mM HEPES, pH 7.2) and intercellular diffusion of 2-NBDG glucose via gap junctions was tested by evaluating its transfer to neighboring cells. Briefly, cells were iontophoretically microinjected with a glass micropipette filled with 20 mM 2-NBDG in recording medium containing 200 μM La^{3+} to avoid cell leakage of the microinjected 2-NBDG via connexin hemichannels, leading to underscore the extent of dye coupling. Fluorescent cells were observed using a Nikon inverted microscope equipped with epifluorescence illumination (Xenon arc lamp) and Nikon B filter to 2-NBDG (excitation wavelength 495 nm; emission wavelength above 505 nm) and XF34 filter to DiI fluorescence (Omega Optical, Inc., Brattleboro, VT, USA). Photomicrographs were obtained using a CCD monochrome camera (CFW-1310 M; Scion; Frederick, MD, USA). Ten minutes after 2-NBDG injection, cells were observed to determine whether 2-NBDG transfer occurred. The coupling index was calculated as the mean number of cells to which the 2-NBDG spread. Three experiments were performed for every treatment and 2-NBDG coupling was tested by microinjecting a minimum of 10 cells per experiment.

2.16. Detection of superoxide anions

Cells plated on glass coverslips were incubated with 0.5 μM MitoSOX Red (ThermoFisher, Carlsbad, CA) for 30 min at 37 °C in Locke's solution (154 mM NaCl, 5.4 mM KCl, 2.3 mM $CaCl_2$, 5 mM HEPES, pH 7.4). After three washes with Locke's solution (154 mM NaCl, 5.4 mM KCl, 2.3 mM CaCl2, 5 mM HEPES, pH 7.4) cells mounted on the stage of an Olympus BX 51W1I upright microscope with a 40× water immersion objective. Images were captured by a Retiga 1300I fast-cooled monochromatic digital camera (12-bit) (Qimaging, Burnaby, BC, Canada) controlled by imaging Metafluor software (Universal Imaging, Downingtown, PA) (exposure time = 0.5 s; excitation and emission wavelengths were 495 nm and 550 nm, respectively). The fluorescence intensity recorded from ≥30 regions of interest (representing at least 30 cells per each image from a total of ≥10 images obtained per each coverslip) was calculated with the following formula: Corrected total cell fluorescence = Integrated Density – ([Area of the selected cell] x [Mean fluorescence of background readings]).

2.17. Cell death

Cell membrane breakdown was evaluated by the incorporation of the cell-impermeant viability indicator Ethidium homodimer-1 (EthD-1). Briefly, cells were incubated with Hank's balanced salt solution with EthD-1 (5 μM) and Hoechst 33342 (1 μM) at 37 °C for 15 min and then washed three times in PBS. Hoechst 33342 and EthD-1 imaging

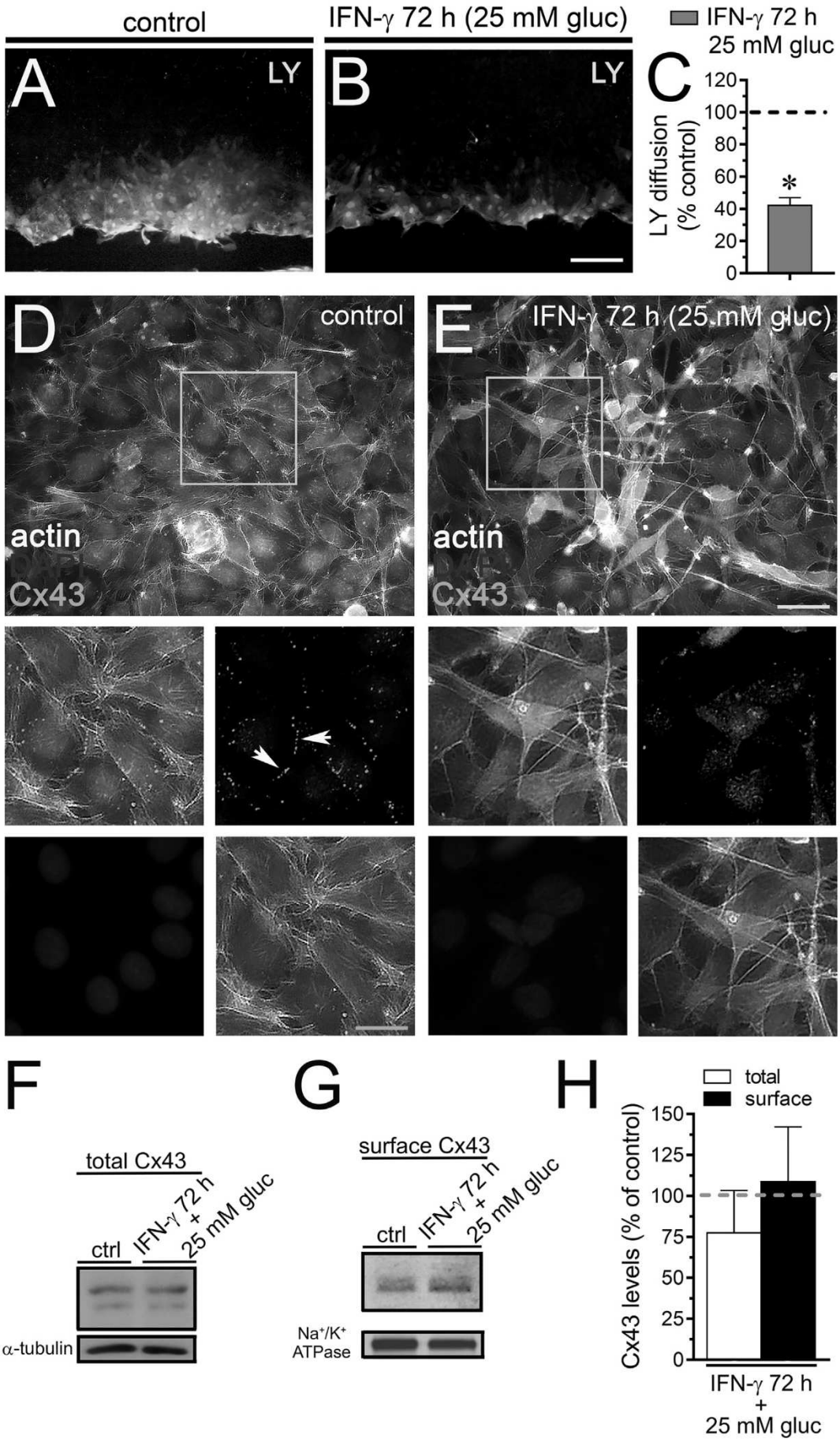

(caption on next page)

Fig. 3. IFN-γ plus high glucose decrease endothelial coupling through a mechanism that involve changes in Cx43 distribution but not changes in its total levels. (**A-B**) Representative fluorescence micrographs of scrape loading/dye transfer assay (SL/DT) with Lucifer yellow (LY) by EAhy cells treated for 72 h with 5 mM glucose (control, **A**) or IFN-γ plus 25 mM glucose (**B**). (**C**) Averaged data normalized to control (dashed line) of SL/DT with LY by EAhy cells treated for 72 h with IFN-γ plus 25 mM glucose. *$p < .05$, IFN-γ plus high glucose compared to control (two-tailed Student's unpaired *t*-test). Data were obtained from at least three independent experiments. White scale bar = 100 μm. (**D–E**) Representative fluorescence images depicting Cx43 (green), phalloidin-actin (white) and DAPI (blue) immunolabeling of EAhy cells treated for 72 h with 5 mM glucose (control, **D**) and IFN-γ plus 25 mM glucose (**E**). Insets: 1.5× magnification of the indicated area of panels **D** and **E**. White arrows indicate Cx43 labeling in cell-cell interfaces. Calibration Bars: yellow = 20 μm, and green = 10 μm. (**F-G**) Relative amount of total (**F**) and surface (**G**) Cx43 in EAhy cells treated for 72 h with 5 mM glucose (control) or IFN-γ plus 25 mM glucose. Total and surface amount of each analyzed band were normalized to the amount of α-tubulin and Na^+/K^+ ATPase detected in each lane, respectively. (**H**) Quantification of total (white bars) and surface (black bars) amount of Cx43 normalized to control (dashed line) in EAhy cells harvested 72 h after treatment with IFN-γ plus 25 mM glucose. Averaged data were obtained from at least three independent experiments.

involved data acquisition (emission at 350 and 528 nm, respectively) at 461 and 628 nm excitation wavelengths, respectively, using an Olympus BX 51W1I upright microscope with a 40× water immersion objective. The quantification of cell death was expressed as the percentage of cells that incorporated EthD-1 (red cells) in relation of total cell population (blue cells) in each image captured. A total of 15 images (20–30 cells per image) for each experiment were analyzed using the ImageJ software.

2.18. Data analysis and statistics

For each data group, results were expressed as mean ± standard error (SEM); n refers to the number of independent experiments. Detailed statistical results were included in the figure legends. Statistical analyses were performed using GraphPad Prism (version 7, GraphPad Software, La Jolla, CA). Normality and equal variances were assessed by the Shapiro-Wilk normality test and Brown-Forsythe test, respectively. Unless otherwise stated, data that passed these tests were analyzed by unpaired *t*-test in case of comparing two groups, whereas in case of multiple comparisons, data were analyzed by one or two-way analysis of variance (ANOVA) followed, in case of significance, by a Tukey's post-hoc test. A probability of $P < 0.05$ was considered statistically significant.

3. Results

3.1. The high glucose-induced activity of Cx43 hemichannels is potentiated by IFN-γ in endothelial cells

In a previous work, we found that IL-1β in combination with TNF-α enhance the activation of Cx43 hemichannels evoked by high glucose in endothelial cells [13]. Because IFN-γ disturbs the morphology and permeability of endothelial cells [11,12], we investigated whether this cytokine could potentiate the hemichannel opening evoked by high glucose in the human endothelial cell line EAhy 926. Time-lapse recording of Etd uptake has been shown to be a reliable strategy to measure the activity of connexin hemichannels [19]. IFN-γ (2.5 ng/ml) potentiated the increase in Etd uptake triggered by 45 mM glucose when compared to 5 mM glucose (hereinafter termed as to "control condition" (Fig. 1A). In addition, 25 mM glucose (henceforward termed as to "high glucose") only raised Etd uptake when was co-incubated with IFN-γ (Fig. 1A–C). The latter effect was time-dependent and peaked at 72 h of treatment (Fig. 1E), whereas no differences were detected with IFN-γ plus high sucrose or mannitol, excluding the action of an osmolarity-mediated response (not shown).

The implication of Cx43 hemichannels in IFN-γ and high glucose-depended Etd uptake was investigated using special mimetic peptides (Tat-L2 and gap19) with sequences equivalent to intracellular L2 loop regions of Cx43 [20,21]. Treatment with Tat-L2 (100 μM) or gap19 (100 μM) completely prevented the Etd uptake induced by IFN-γ plus high glucose (Fig. 1E). Similar inhibitory responses were found with gap27 (100 μM), a mimetic peptide against the second extracellular loop of Cx43 [22] or La^{3+} (200 μM) [23], a general inhibitor of connexin hemichannels (Fig. 1E). Of note, both a mutated Tat-L2 (100 μM Tat-$L2^{H126K/I130N}$), in which 2 amino acids pivotal for the interaction of L2 region to the carboxyl tail of Cx43 are changed, or an inactive type of gap19 enclosing the I130A variation (gap19^{I130A}), failed in evoking comparable preventive effects (Fig. 1E). In line with these results, downregulation of Cx43 with siRNA totally abrogated the Etd uptake induced by IFN-γ plus high glucose (Fig. 1E). Other routes that may account for the Etd uptake of endothelial cells are plasma membrane channels formed by pannexin-1 (Panx1) [24–27]. Unlike what was seen upon Cx43 blockade, scrambled Cx43 siRNA, siRNA for Panx1, the Panx1 mimetic peptide ^{10}panx1 (100 μM) or probenecid (200 μM) did not reduce the Etd uptake triggered by IFN-γ plus high glucose (Fig. 1E).

To further corroborate the stimulatory action of IFN-γ plus high glucose on Cx43 hemichannel activity, whole-cell voltage-clamp experiments were performed along with recordings of macroscopic membrane currents (Fig. 1F–I). In control EAhy cells unitary current transitions were almost undetected at resting potentials (Fig. 1F), whereas the treatment with IFN-γ plus high glucose for 72 h induced the appearance of several discrete unitary current events (Fig. 1F). Moreover, the macroscopic currents evoked by IFN-γ plus high glucose were strongly inhibited by two Cx43 hemichannel inhibitors: La^{3+} or gap27 (Fig. 1H,I). Overall, these findings reveal that IFN-γ plus high glucose prominently augment the activity of Cx43 hemichannels in endothelial cells.

3.2. IL-1β/TNF-α/p38 MAPK/iNOS/COX_2/EP_1–associated pathways and the $P2X_7$/$P2Y_1$/IP_3 receptor-dependent changes in cytoplasmic Ca^{2+} are crucial for the endothelial Cx43 hemichannel activity induced by IFN-γ plus high glucose

Previous evidence has pointed out that different inflammatory mediators and signaling proteins are involved in the activation of Cx43 hemichannels during pathological conditions, including TNF-α, IL-1β, p38 MAPK, the iNOS, COX_2, NO, and prostaglandins [13,28–32].. From this perspective, we tested the impact of these elements on the IFN-γ and high glucose-dependent Etd uptake in EAhy cells. Inhibition of IL-1β/TNF-α signaling with a soluble form of TNF-α receptor that binds TNF-α (sTNF-aR1) and/or a recombinant antagonist for the IL-1β receptor (IL-1ra) strongly counteracted the IFN-γ and high glucose-evoked Etd uptake (Fig. 2). Potent inhibitory effects were also found upon blockade of p38 MAPK, iNOS and COX_2 with SB202190 (10 μM), L-N6 (5 μM) and ns-398 (5 μM), respectively (Fig. 2). The general antagonist of COX_1 and COX_2 indomethacin (15 μM) partially decreased the raise on Etd uptake promoted by IFN-γ and high glucose, whereas the selective COX1 blocker sc-560 (1 μM) failed in induce a similar response (Fig. 2). [33,34] The activation of EP_1 receptors and subsequent raise in cytoplasmic Ca^{2+} have been linked with the inflammatory-induced opening of Cx43 hemichannels in astrocytes, microglia and endothelial cells [13,35,36]. In view of this, we studied whether these pathways are implicated in our system. sc-19,220 (20 μM), a specific EP_1 receptor antagonist, and 5 μM BAPTA-AM, a Ca^{2+} chelator, strongly reduced the Etd uptake triggered by IFN-γ plus high glucose (Fig. 2). Multiple mechanisms have been associated with the $[Ca^{2+}]_i$-dependent Cx43 hemichannel opening, such as the

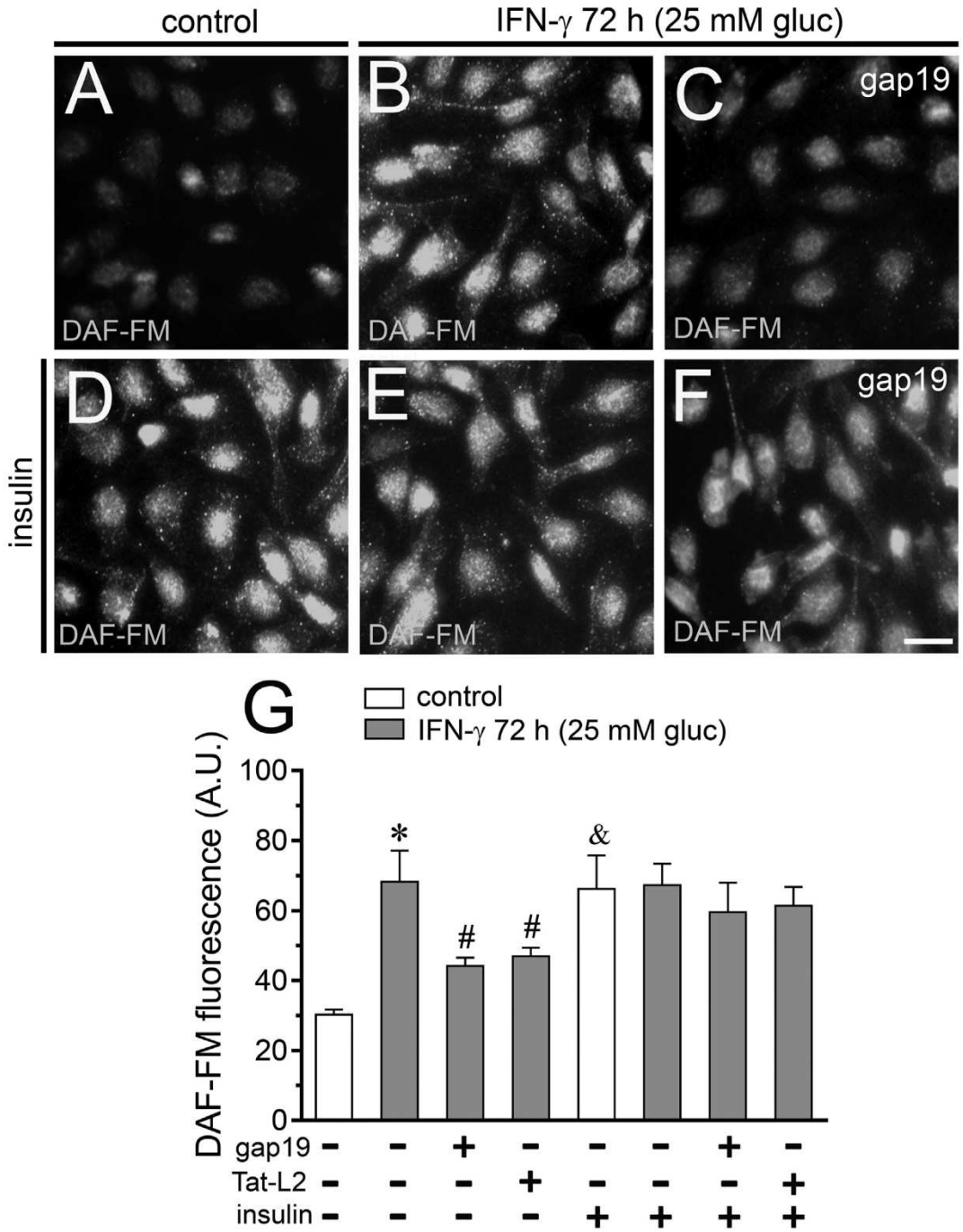

Fig. 4. IFN-γ plus high glucose increases basal but not insulin-induced production of NO in endothelial cells: prevention by Cx43 hemichannel blockers. (**A-F**) Representative fluorescence micrographs of basal (**A-C**) or 1 μM insulin-induced (**D-F**) production of NO (DAF-FM, green and pseudo-colored scale) of EAhy cells treated for 72 h with 5 mM glucose (control; **A, D**), IFN-γ plus 25 mM glucose (**B, E**) alone or in combination with 100 μM gap19 (**C, F**). (**G**) Average of DAF fluorescence by EAhy cells treated for 72 h with 5 mM glucose (control; white bars), IFN-γ plus 25 mM glucose (blue bars) alone or with different combinations of the following compounds: 1 μM insulin, 100 μM gap19 or 100 μM Tat-L2. $^{*}p < .05$, IFN-γ plus high glucose compared to control; $^{\#}p < .05$, effect of each compound compared to the effect induced by IFN-γ and high glucose; $^{\&}p < .05$, effect of insulin compared to the respective control (one-way ANOVA followed by Tukey's post-hoc test). Data were obtained from at least three independent experiments with four repeats each one (≥35 cells analyzed for each repeat). Calibration Bar = 10 μm.

signaling via ryanodine receptors, αvβ3 integrin and purinergic receptors [37–39]. To examine the latter possibility, we investigate whether purinergic signaling take part in the IFN-γ and high glucose-dependent Etd uptake in EAhy cells. Neutralization of $P2X_7$ receptors with 200 μM oATP or 10 μM A740003, significantly abrogated the Etd uptake triggered by IFN-γ and high glucose, whereas inhibition of $P2Y_1$ receptors, phospholipase C (PLC) or IP_3 receptors with 10 μM MRS2179, 5 μM U73122 or 50 μM APB, respectively, caused an equivalent inhibitory impact (Fig. 2). Collectively, these findings support the fact that activation of IL-1β/TNF-α/p38 MAPK/iNOS/COX_2/EP_1–dependent pathway(s) and the $P2X_7$/$P2Y_1$/IP_3 receptor-mediated changes in cytoplasmic Ca^{2+} signal are critical for endothelial Cx43 hemichannel activity triggered by IFN-γ plus high glucose.

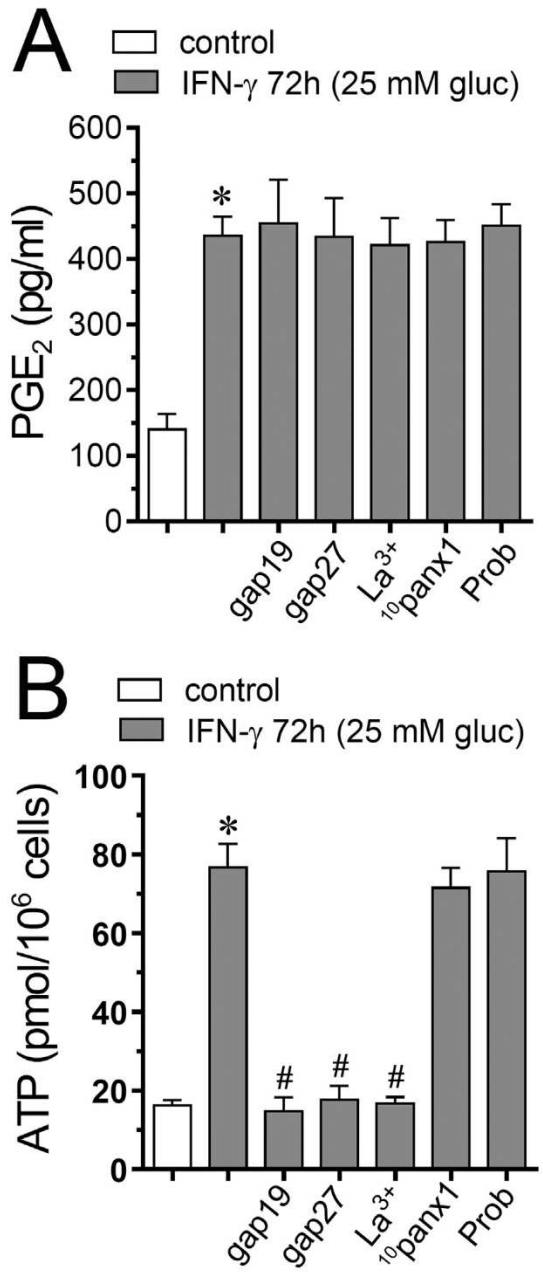

Fig. 5. IFN-γ plus high glucose induces the release of PGE_2 and ATP, the latter being dependent on the activation of Cx43 hemichannels in endothelial cells. (**A-B**) Averaged data of PGE_2 (**A**) or ATP (**B**) release from EAhy cells treated for 72 h with 5 mM glucose (control, white bar), IFN-γ plus 25 mM glucose (blue bars) alone or in combination with the following agents: 100 μM gap19, 100 μM gap27, 200 μM La^{3+}, 100 μM ^{10}panx1 or 500 μM Probenecid (Prob). *$p < .05$, IFN-γ plus high glucose compared to control; $^{\#}p < .05$, effect of each agent compared to the effect induced by IFN-γ plus high glucose (one-way ANOVA followed by Tukey's post-hoc test). Data were obtained from at least three independent experiments with four repeats each one.

3.3. IFN-γ plus high glucose reduces gap junctional communication but do not affect the surface amount of Cx43 hemichannels in endothelial cells

Diverse research groups have found that inflammatory conditions increase the activity of connexin hemichannels in concomitance with a reduction in gap junctional communication [40,41], not being endothelial cells an exception [13]. In line with this, we found that IFN-γ plus high glucose induced a ~60% reduction on gap junction-mediated coupling in EAhy cells, as measured by LY intercellular diffusion (Fig. 3A–C). The functional state of gap junctions can be modulated by changes in the open probability, single channel conductance or selectivity, as well as changes in the number of channels found at cell-cell interfaces [42]. Accordingly, we examined whether modifications in allocation of Cx43 may account for the IFN-γ and high glucose-induced reduction in gap junctional communication observed in endothelial cells. As previously reported [13], in control cells Cx43 was localized mostly and intensely as fine to large dots scattered at cell–cell interfaces (Fig. 3D). In contrast, the latter was not detected in endothelial cells treated for 72 h with IFN-γ and high glucose, where Cx43 was found in numerous intracellularly and perinuclear vesicle-like structures (Fig. 3E). Altogether this evidence suggests that withdrawal of Cx43 gap junctions found at appositional membranes could be sufficient to explain the IFN-γ and high glucose-induced endothelial uncoupling.

To scrutinize whether similar modifications in the number of channels could explain the Etd uptake observed in endothelial cells, we measured surface levels of Cx43 hemichannels via cell surface biotinylation of membrane proteins. IFN-γ plus high glucose failed in to alter either the total or surface Cx43 amount when compared to control conditions (Fig. 3E–G). Furthermore, the pattern of immunoreactive bands of Cx43 was not affected, indicating the absence of modifications in the phosphorylation state of Cx43 detectable by alterations in electrophoretic mobility (Fig. 3E–G). Therefore, the IFN-γ and high glucose-induced Cx43 hemichannel activity may occur by a mechanism different from increments in surface amount of Cx43 hemichannels.

3.4. IFN-γ plus high glucose impair the insulin-dependent increase in NO production in endothelial cells

. Given that the inhibition of iNOS greatly abrogated the IFN-γ and high glucose-induced Etd uptake in EAhy cells (Fig. 2) and because impairment of NO production occurs in diabetes and atherosclerosis [43], we evaluated the amount of this molecule in our system. IFN-γ plus high glucose caused a ~2.2-fold increase in basal NO production in relation to control conditions, as detected through analysis of DAF fluorescence signal (Fig. 4A, B and G). In a previous work, we found that IL-1β/TNF-α plus high glucose potentiates NO production induced by insulin. In order to examine whether IFN-γ plus high glucose could evoke similar effects, we studied the insulin-induced production of NO. Contrary to what occurred in control conditions, insulin did not increase the NO amount in cells treated with IFN-γ plus high glucose (Fig. 4D, E and G). Moreover, although 100 μM gap19 or 100 μM Tat-L2 partially abolished the IFN-γ and high glucose-mediated NO production, both inhibitors failed to induce a similar response in cells treated with IFN-γ plus high glucose and exposed to insulin (Fig. 4F and G). Collectively, these results indicate that IFN-γ plus high glucose increase the amount of NO, being the activation of Cx43 hemichannels crucial in this cell response. In contrast, treatment with IFN-γ plus high glucose impedes the increase in the amount of NO evoked by insulin through a mechanism different from opening of Cx43 hemichannels.

3.5. IFN-γ plus high glucose triggers the release of PGE_2 and ATP from endothelial cells

Prior studies have reported that NO-dependent stimulation of COX_2 may lead to the production of PEG_2 and further activation of EP_1 receptor [33,34]. Because this receptor participates in the activity of Cx43 hemichannels in our system (Fig. 2) and in other pathological conditions [13,35], we studied whether IFN-γ plus high glucose could alter the release of PGE_2 from endothelial cells. Endothelial cells treated with IFN-γ plus high glucose displayed a ~3-fold increase in the release of PGE_2 in relation to control conditions, being this response not sensitive to the blockade of Cx43 hemichannels or Panx1 channels (Fig. 5A). During pathological conditions, ATP is one of the paracrine signals released through Cx43 hemichannels in different cell types [44], including endothelial [13,45,46]. Given that $P2X_7$ and $P2Y_1$ receptors

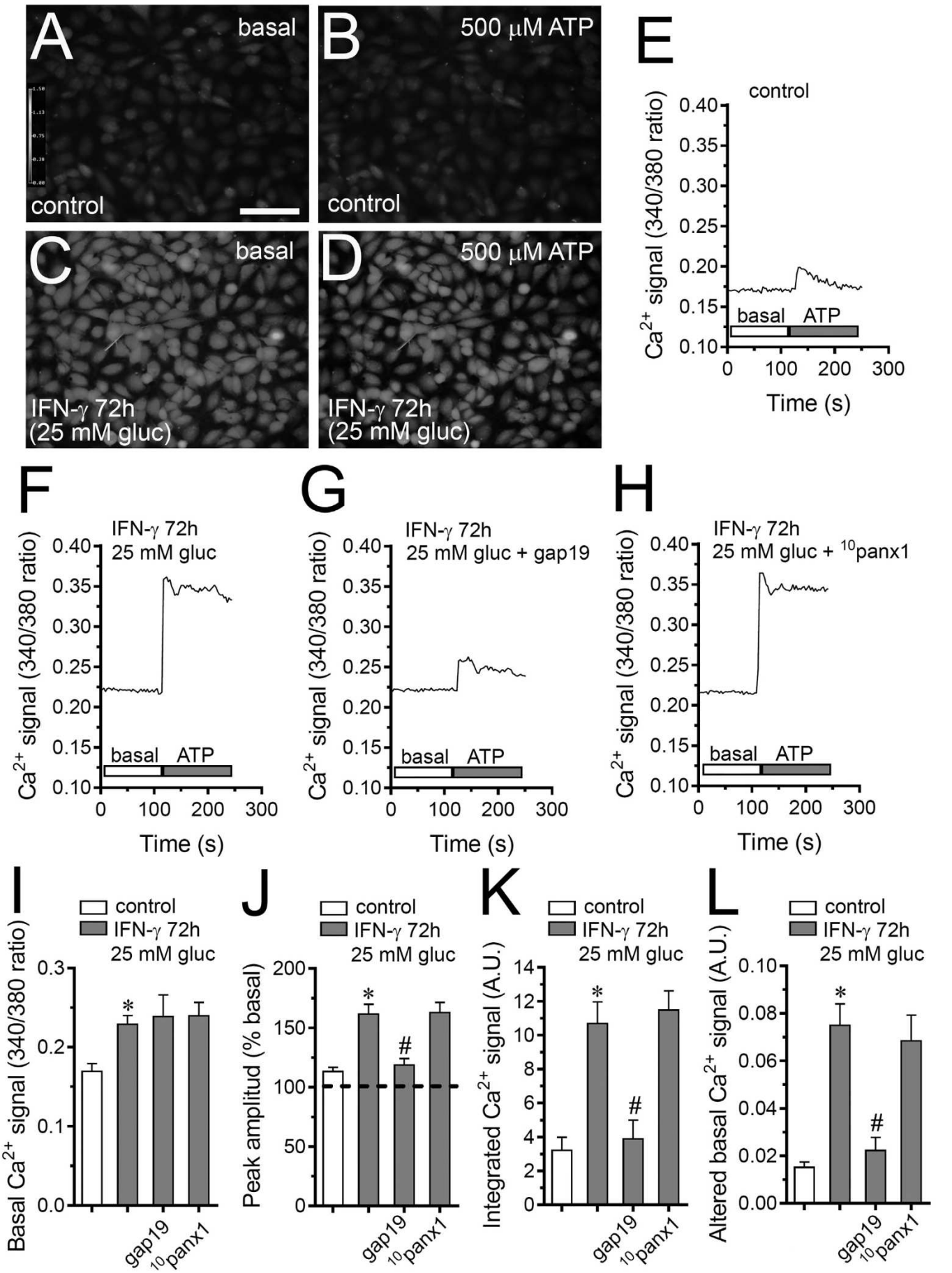

(caption on next page)

Fig. 6. IFN-γ plus high glucose augments basal and ATP-dependent Ca^{2+} dynamics in endothelial cells: prevention by Cx43 hemichannel blockers. (**A-D**) Representative photomicrographs of basal (**A**, **C**) or 500 μM ATP-induced (**B**, **D**) Ca^{2+} signal denoted as Fura-2 ratio (340/380 nm excitation) of EAhy cells treated for 72 h with 5 mM glucose (control; **A**, **B**) or IFN-γ plus 25 mM glucose (**C**, **D**). Calibration bar: 40 μm. (***E*-H**) Representative plots of relative changes in Ca^{2+} signal over time induced by 500 μM ATP (green horizontal line) in EAhy cells treated for 72 h with 5 mM glucose (control, **E**), IFN-γ plus 25 mM glucose (**F**) alone or in combination with 100 μM gap19 (**G**) or 100 μM ^{10}panx1 (**H**). (**I**) Averaged data of basal Fura-2 AM ratio by EAhy cells treated for 72 h with 5 mM glucose (control, white bar), IFN-γ plus 25 mM glucose and (blue bars) alone or in combination with 100 μM gap19 or 100 μM ^{10}panx1. (**J-L**) Averaged data of ATP-induced peak amplitude normalized to basal Fura-2 AM ratio (**J**), integrated ATP-induced Fura-2 AM ratio response (**K**) and altered basal Fura-2 AM ratio (**L**) of EAhy cells treated for 72 h with 5 mM glucose (control, white bar), IFN-γ plus 25 mM glucose (blue bars) alone or in combination with 100 μM gap19 or 100 μM ^{10}panx1. *$p < .05$, IFN-γ plus high glucose compared to control; $^{\#}p < .05$, effect of each pharmacological agent compared to the effect induced by IFN-γ plus high glucose (one-way ANOVA followed by Tukey's post-hoc test). Data were obtained from at least three independent experiments with four repeats each one (≥35 cells analyzed for each repeat).

were involved in the activity of Cx43 hemichannels in our system (Fig. 2), we tested the release of this molecule. The extracellular ATP concentration was increased in ~5-folds upon treatment with IFN-γ plus high glucose (Fig. 5B). Unlike to what observed with the release of PGE_2, gap19, gap27 and La^{3+}, but not ^{10}panx1 or probenecid, totally blunted the release of ATP promoted by IFN-γ plus high glucose (Fig. 5B), suggesting the engagement of Cx43 hemichannels in this process.

3.6. IFN-γ plus high glucose augments ATP-dependent Ca^{2+} dynamics in endothelial cells

The activation of EP_1 receptors induces the rise of cytoplasmic Ca^{2+} [47] and the latter is a well-known response that augments the open probability of Cx43 hemichannels [48], resulting in increased ATP release [39]. With this antecedent and because cytoplasmic Ca^{2+} and purinergic signaling underpin the IFN-γ and high glucose-dependent Etd uptake (Fig. 2), we evaluated if this treatment could alter the basal and ATP-induced Ca^{2+} signal in EAhy cells. IFN-γ plus high glucose induced a significant increase (~30%) in basal Ca^{2+} signal when compared to control conditions, as measured by analysis of Fura-2 ratio (340/380) (Fig. 6A, C and I). Upon 500 μM ATP application, control endothelial cells responded with a fast and transient Ca^{2+} signal characterized by a small amplitude, whereas IFN-γ and high glucose-treated cells showed a sustained response with a peak ~6-fold bigger than of control values (Fig. 6D, F and J). IFN-γ plus high glucose also elevated in ~3.2-fold and ~5.5-fold the integrated ATP-dependent Ca^{2+} signal response (Fig. 6K) and the remaining difference between final and initial basal Ca^{2+} signal (Fig. 6L), respectively. Relevantly, we found that inhibition of Cx43 hemichannels with gap19 fully counteracted the increase in ATP-mediated Ca^{2+} peak but not basal Ca^{2+} signal induced by treatment with IFN-γ plus high glucose (Fig. 6I and J). Similarly, the blockade of Cx43 hemichannels fully prevented the raise in the integrated area under curve and remaining basal ATP-dependent Ca^{2+} signal responses caused by IFN-γ plus high glucose (Fig. 6K and L). In contrast, inhibition of Panx1 channels with ^{10}panx1 failed in cause similar preventive effects (Fig. 6K and L). Therefore, these data indicate that elevated Cx43 hemichannel activity participates in the IFN-γ and high glucose-induced increase in ATP-mediated Ca^{2+} signaling in endothelial cells.

3.7. IFN-γ plus high glucose impairs the insulin-dependent uptake and intercellular diffusion of glucose in endothelial cells via the activation of Cx43 hemichannels

Accumulating evidence has demonstrated that inflammatory mediators impair both insulin signaling and glucose uptake in endothelial cells [49,50], which are pivotal pieces in the progression of diabetes and atherosclerosis [51]. To further scrutinize more deeply the effect of IFN-γ plus high glucose in the impaired response of endothelial cells to insulin, we explored the impact of this treatment on the insulin-induced uptake of 2-NBDG, a fluorescent glucose analogue. Experiments of 2-NBDG uptake uncovered that basal glucose uptake remains unchanged upon treatment with IFN-γ plus high glucose in EAhy cells (Fig. 7A, B and G). However, exposure for 30 min with 1 μM insulin evoked ~40% augment in glucose uptake in control conditions (Fig. 7D and G). Noteworthy, treatment with IFN-γ plus high glucose made endothelial cells insensitive to insulin, showing levels of glucose uptake indistinguishable from those of control cells that were not stimulated with insulin (Fig. 7E and G). More relevant to this point, treatment with 100 μM gap19 or 100 μM Tat-L2 dramatically prevented the above response and did not modulate basal glucose uptake in control cells (Fig. 7C, F and G).

It is known that intercellular diffusion of glucose take place through gap junctions in different cell types including astrocytes, oligodendrocytes and cells of the cochlea [52–55]. In this context, we tested whether IFN-γ plus high glucose could modulate the intercellular diffusion of 2-NBDG in basal conditions or after insulin stimulation. Under control conditions, EAhy cells were largely coupled to 2-NBDG (~20 cells) (Fig. 8A and G). However, the treatment with IFN-γ plus high glucose reduced ~50% this response (Fig. 8B and G). Notably, blockade of Cx43 hemichannels with gap19 totally prevented the uncoupling effect caused by IFN-γ plus high glucose (Fig. 8C and G). Control cells incubated with 1 μM insulin for 30 min showed ~60% increase in 2-NBDG intercellular transfer (Fig. 8D and G). Of note, similar to what was observed with glucose uptake, IFN-γ plus high glucose totally counteracted the effects of insulin and consequently the intercellular transfer of 2-NBDG was prominently reduced (Fig. 8E and G). Interesting was the fact that gap19 fully prevented this inhibitory effect (Fig. 8F and G). Overall, these data suggest that IFN-γ plus high glucose impairs the insulin effects on the uptake and intercellular transfer of 2-NBDG by a process implicating the activation of Cx43 hemichannels.

3.8. IFN-γ plus high glucose increases superoxide levels and cell death in endothelial cells by a mechanism implicating the activity of Cx43 hemichannels

IFN-γ or high glucose increase the production of reactive oxygen species (ROS) and impair mitochondrial function in endothelial cells [56–58]. With this in mind and because Cx43 hemichannel opening alters intracellular oxidative status [59], we evaluated if IFN-γ plus high glucose could modulate the production of superoxide anion by the mitochondria via the activation of Cx43 hemichannels. Accordingly, we measured the production of mitochondrial superoxide by using the fluorescent probe MitoSOX red. Control EAhy cells displayed almost undetectable signal of superoxide anion (Fig. 9A, D and G), whereas those stimulated with IFN-γ plus high glucose showed ~10-fold increase in the production of this free radical (Fig. 9B, E and G). Noteworthy, both gap19 or Tat-L2 fully blunted the increase in superoxide anion signal triggered by IFN-γ plus high glucose (Fig. 9C, F and G), suggesting that Cx43 hemichannels critically contribute to this response.

Different lines of evidence have described that both IFN-γ or high glucose trigger endothelial cell death [60–62], whereas the persistent activation of Cx43 hemichannels appear to be essential for inducing cell death in different cell types [35,63,64]. Taking this into account, we evaluated if IFN-γ plus high glucose could induce endothelial cells death by a mechanism implicating the opening of Cx43 hemichannels.

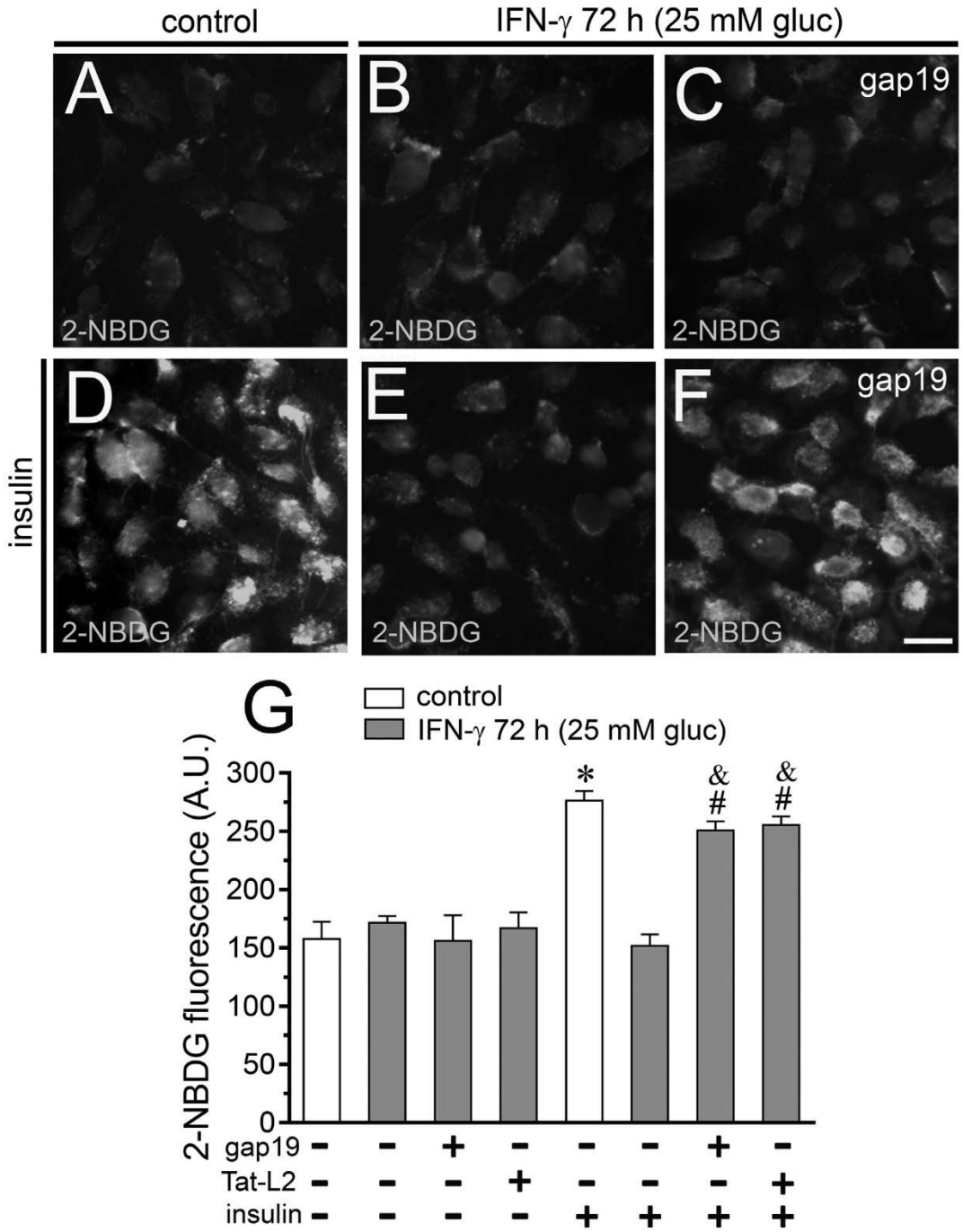

Fig. 7. IFN-γ plus high glucose impedes the insulin-induced uptake of glucose in endothelial cells: prevention by Cx43 hemichannel blockers. (**A**-**F**) Representative fluorescence micrographs of basal (**A-C**) or 1 μM insulin-induced (**D-F**) uptake of 2-NBDG glucose (green) of EAhy cells treated for 72 h with 5 mM glucose (control; **A, D**), IFN-γ plus 25 mM glucose (**B, E**) alone or in combination with 100 μM gap19 (**C, F**). (**G**) Average of 2-NBDG glucose uptake by EAhy cells treated for 72 h with 5 mM glucose (control; white bars), IFN-γ plus 25 mM glucose (blue bars) alone or with different combinations of the following compounds: 1 μM insulin, 100 μM gap19 or 100 μM Tat-L2. *$p < .05$, IFN-γ plus high glucose compared to control; $^{\#}p < .05$, effect of each compound compared to the effect induced by IFN-γ and high glucose; $^{\&}p < .05$, effect of each compound compared to the effect induced by IFN-γ, high glucose and insulin (one-way ANOVA followed by Tukey's post-hoc test). Data were obtained from at least three independent experiments with four repeats each one (≥35 cells analyzed for each repeat). Calibration Bar = 10 μm.

Consequently, we analyzed the incorporation of EthD-1, a molecule that due to its large size is taken up only by cells with disrupted membranes, thereby, it is indicative of loss of membrane integrity. The vast majority of control EAhy cells did not incorporate EthD-1 (Fig. 10A and D). Nonetheless, treatment with IFN-γ plus high glucose triggered a time-dependent increase in cell death, being 6 days post-treatment the most significant as it was found ~20% of damage in relation to control condition (Fig. 10B and D). Notably, endothelial cell damage evoked by 6 days of incubation with IFN-γ plus high glucose was prominently counteracted by diverse Cx43 hemichannels blockers including gap19, gap27, Tat-L2 and La^{3+} (Fig. 10C and E). In general, these evidences argue for a crucial role of Cx43 hemichannels on the IFN-γ and high glucose-induced death in endothelial cells.

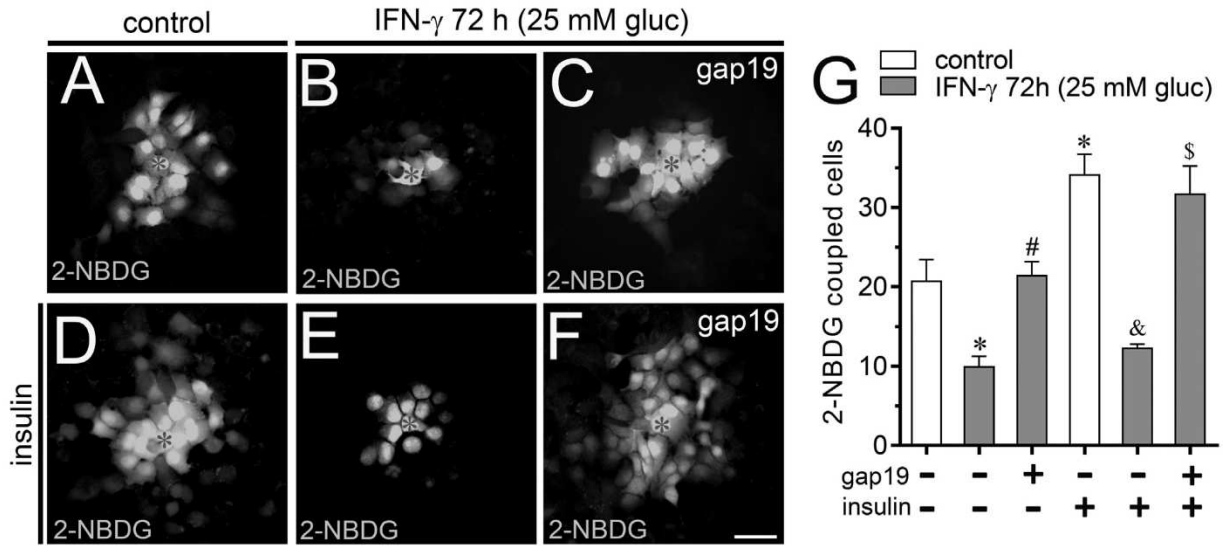

Fig. 8. IFN-γ plus high glucose prevents the basal and the insulin-induced intercellular diffusion of glucose in endothelial cells: prevention by Cx43 hemichannel blockers. (**A-F**) Representative fluorescence micrographs of basal (**A-C**) or 1 μM insulin-induced (**D-F**) intercellular diffusion uptake of 2-NBDG glucose (green) of EAhy cells treated for 72 h with 5 mM glucose (control; **A, D**), IFN-γ plus 25 mM glucose (**B, E**) alone or in combination with 100 μM gap19 (**C, F**). (**G**) Average of the number of EAhy cells coupled to 2-NBDG glucose after treatment for 72 h with 5 mM glucose (control; white bars), IFN-γ plus 25 mM glucose (blue bars) alone or with different combinations of the following compounds: 1 μM insulin or 100 μM gap19. *$p < .05$, IFN-γ plus high glucose compared to control; $^{\#}p < .05$, effect of each compound compared to the effect induced by IFN-γ and high glucose; $^{\&}p < .05$, effect of IFN-γ plus high glucose plus insulin compared to control plus insulin; $^{\$}p < .05$, effect of gap19 plus insulin compared to the effect of IFN-γ plus high glucose plus insulin (one-way ANOVA followed by Tukey's post-hoc test). Data were obtained from at least three independent experiments with four repeats each one (≥35 cells analyzed for each repeat). Calibration Bar = 35 μm.

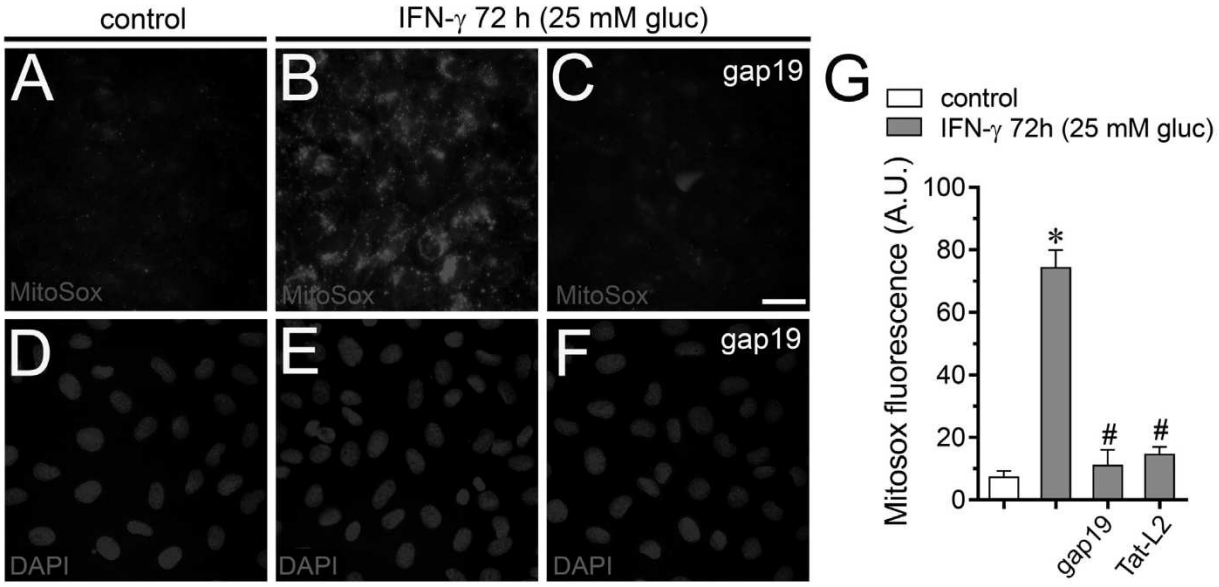

Fig. 9. IFN-γ plus high glucose increases the production of superoxide anion by mitochondria in endothelial cells: prevention by Cx43 hemichannel blockers. (**A-F**) Representative fluorescence micrographs of MitoSOX Red signal (red, **A-C**) and DAPI nuclear staining (blue, **D-F**) by EAhy cells treated for 72 h with 5 mM glucose (control; **A, D**), IFN-γ plus 25 mM glucose (**B, E**) alone or in combination with 100 μM gap19 (**C, F**). (**G**) Average of MitoSox fluorescence by EAhy cells treated for 72 h with 5 mM glucose (control, white bar), IFN-γ plus 25 mM glucose (blue bars) alone or with the following compounds: 100 μM gap19 or 100 μM Tat-L2. *$p < .05$, IFN-γ plus high glucose compared to control; $^{\#}p < .05$, effect of each compound compared to the effect induced by IFN-γ plus high glucose (one-way ANOVA followed by Tukey's post-hoc test). Data were obtained from at least three independent experiments with four repeats each one (≥35 cells analyzed for each repeat). Calibration Bar = 15 μm.

4. Discussion

The present study shows data describing that IFN-γ in combination with a high glucose concentration increases the activity of Cx43 hemichannels in cultured endothelial cells. The functional state of hemichannels was examined by analyzing the Etd uptake in time-lapse recordings of live cells. The use of selective mimetic peptides (Tat-L2, gap19 and gap27) or siRNA known to antagonize Cx43 hemichannels or knock down Cx43, respectively, confirmed the contribution of Cx43 hemichannels to the IFN-γ and high glucose-evoked Etd uptake. The latter was corroborated with electrophysiological experiments in whole-cell configuration, in where both gap27 or La^{3+} entirely suppressed the Cx43 hemichannel currents promoted by IFN-γ and high glucose. These findings are in agreement with a previous study of our group, in where was demonstrated that opening of Cx43 hemichannels evoked by high glucose is potentiated by IL-1β and TNF-α in

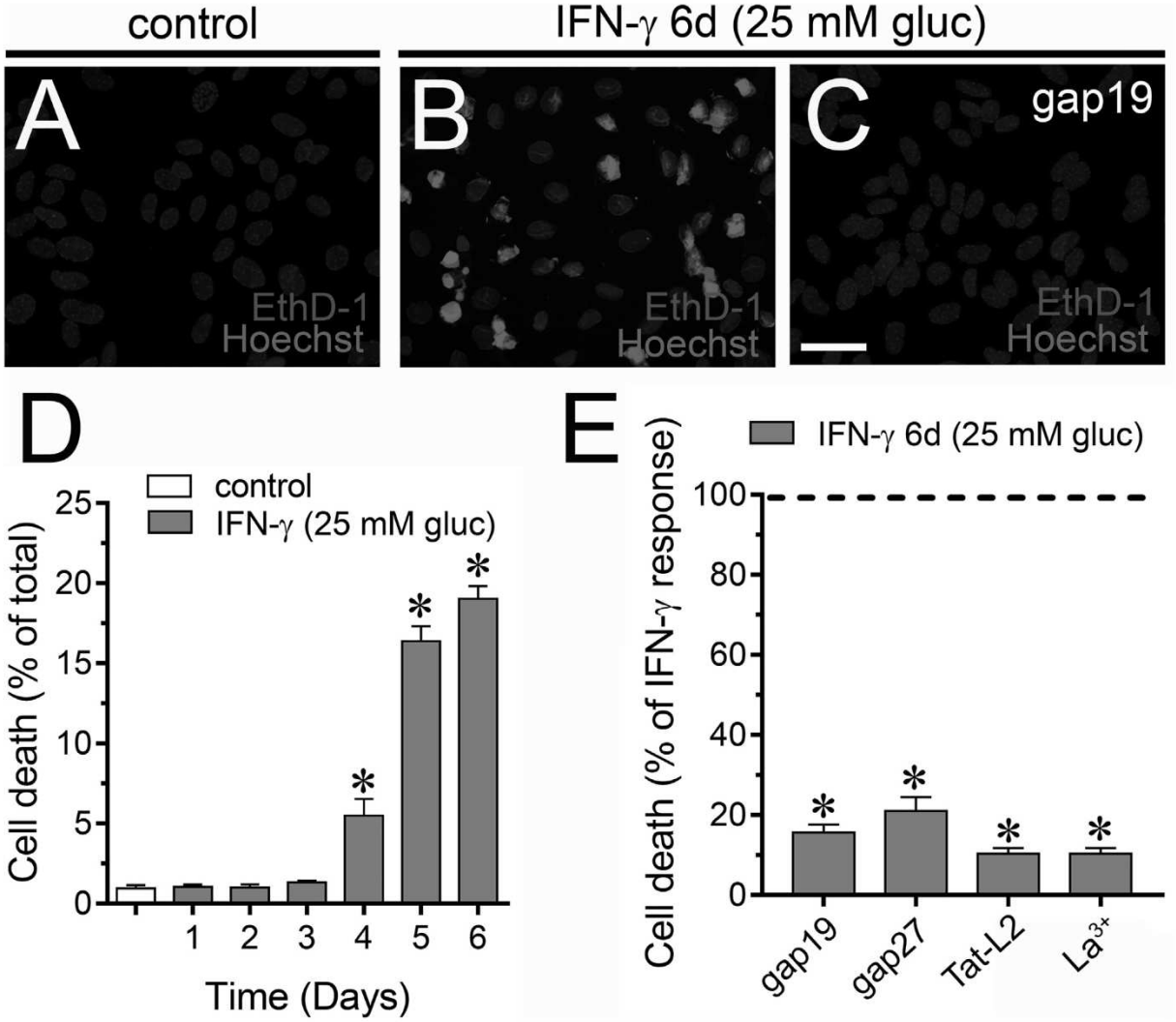

Fig. 10. Cx43 hemichannels contribute to the IFN-γ and high glucose-induced endothelial cell death. (**A-C**) Representative fluorescence micrographs of Eth-D1 (red) uptake and Hoechst 33342 nuclear staining (blue) by EAhy cells treated for 6 days with 5 mM glucose (control; **A**), IFN-γ plus 25 mM glucose (**B**) alone or in combination with 100 μM gap19 (**C**). (**D**) Quantitation of cell death measured by Eth-D1 staining as percentage of total cells identified with Hoechst 33342 by EAhy cells treated with 5 mM glucose (control; white bar) or treated for 1, 2, 3, 4, 5 or 6 days with IFN-γ plus 25 mM glucose (blue bars). (**E**) Averaged data normalized to the effect induced by 6 days of treatment with IFN-γ plus 25 mM glucose on cell death measured by Eth-D1 staining in EAhy cells treated with 100 μM gap19, 100 μM gap27, 100 μM Tat-L2 or 200 μM La^{3+}. *$p < .01$, effect of pharmacological agents compared to IFN-γ plus 25 mM glucose treatment (one-way ANOVA followed by Tukey's post-hoc test). Data were obtained from at least three independent experiments with three or more repeats each one. Calibration bar = 25 μm.

endothelial cells [13]. Although this concordance could seem trivial as all these cytokines are released during pathological conditions, diverse antecedents indicate that IFN-y may act in the opposite manner or synergistically to the signaling of IL-1β or TNF-α depending on the context [65–69]. Supporting the latter possibility, we found that increase in Cx43 hemichannel activity triggered by IFN-γ plus high glucose engages the participation of both IL-1β and TNF-α and their downstream signaling linked to the activation of p38 MAPK and iNOS, as it has been previously shown in astrocytes [28–30].

In both astrocytes and endothelial cells, the increase in Cx43 hemichannel activity evoked by inflammation requires the activation of COXs and PGE_2 receptor EP_1 [13,35]. Crucial for the stimulation of COXs is the iNOS-dependent generation of NO [70]. In harmony with these antecedents, we observed that IFN-γ plus high glucose strongly elevated NO production in EAhy cells, whereas the pharmacological inhibition of COX_2 or EP_1 receptors strongly suppressed the increase in Cx43 hemichannel activity. More relevant to this point, IFN-γ plus high glucose dramatically augmented extracellular amount of PGE_2, which could explain the increase in Cx43 hemichannel activity, as this prostaglandin is critical for $[Ca^{2+}]_i$ responses induced by EP_1 receptors [47], while hemichannels are opened by rise in cytoplasmic Ca^{2+} [48]. Consistent with this notion, IFN-γ plus high glucose increased basal cytoplasmic Ca^{2+} and their stimulatory effect on Cx43 hemichannels was greatly counteracted by intracellular BAPTA.

Accumulating research has pointed out that elevated hemichannel activity lead to cellular damage by multiple mechanisms, including the overload of $[Ca^{2+}]_i$, transmembrane ionic imbalance and release of potential "danger" signals, such as ATP [14,71]. In this line, we found that IFN-γ plus high glucose prominently boosted the Cx43 hemichannel-dependent release of ATP, while inhibition not only of $P2X_7$ and $P2Y_1$ receptors but also PLC or IP_3 receptors strongly suppressed the activation of Cx43 hemichannels. This harmonizes with prior studies showing that Cx43 hemichannels are permeable to ATP [72], which induces its own release via these channels through the activation of purinergic receptors and subsequent rise in $[Ca^{2+}]_i$ [29,73,74]. The latter is in accordance with the fact that moderate rise in $[Ca^{2+}]_i$ (> 500 nM) augments the open probability of Cx43 hemichannels [21,48,75]. In view of this, Cx43 hemichannels could be involved

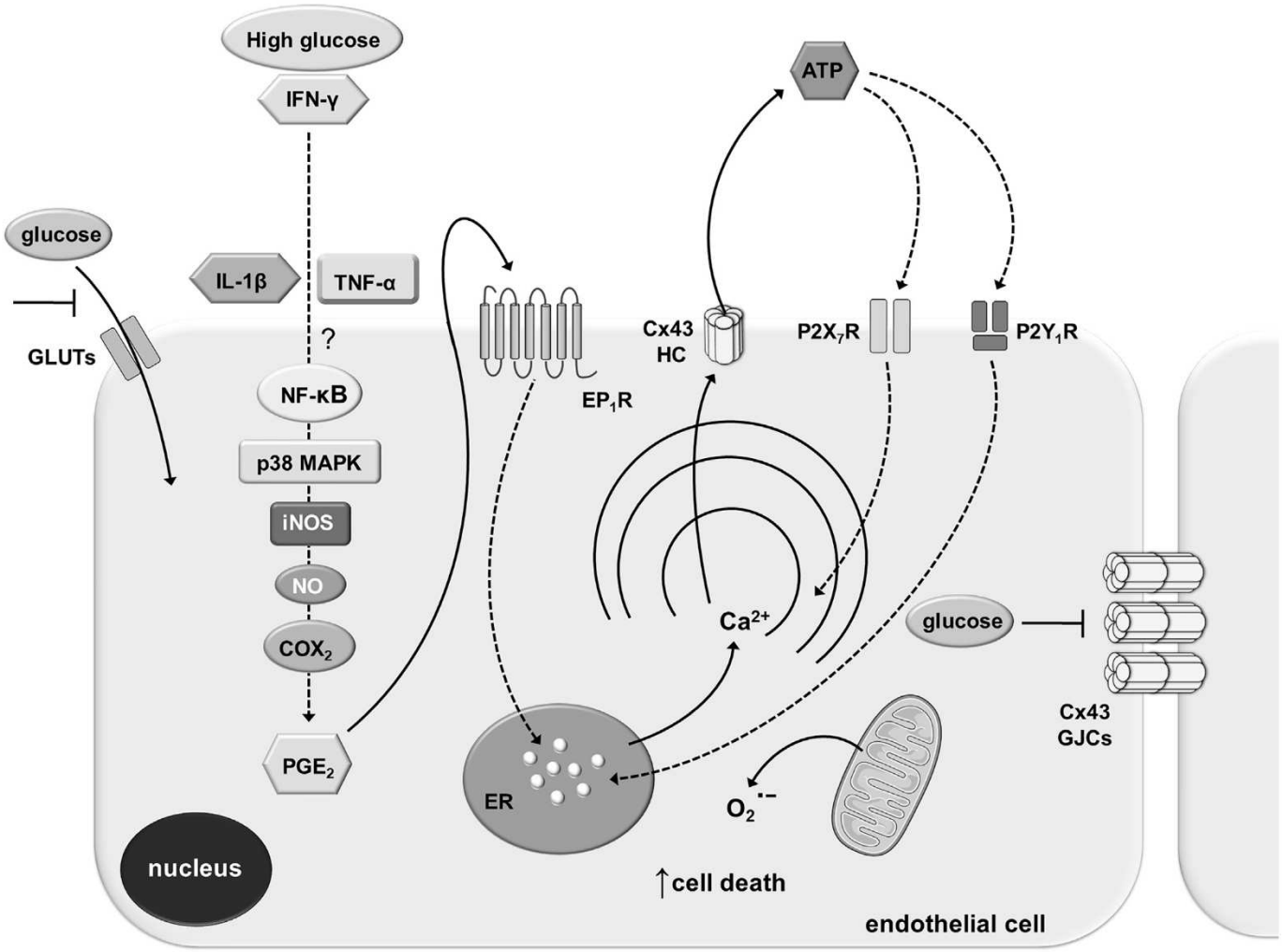

Fig. 11. Schematic diagram illustrating the possible signaling elements involved in the activation of Cx43 hemichannels elicited by high glucose and IFN-γ in endothelial cells. High glucose and IFN-γ induce the production of IL-1β and TNF-α, promoting the p38 MAPK and iNOS activation, NO production and subsequent stimulation of COX_2. This results in the generation of PGE_2, which operating on EP_1 metabotropic receptors, elicits the release of Ca^{2+} from intracellular stores. Moderated increase in $[Ca^{2+}]_i$ augments the activity of Cx43 hemichannels allowing the release of ATP and further activation of $P2X_7$ and $P2Y_1$ receptors. The latter may induce a self-perpetuating mechanism characterized by the influx of extracellular Ca^{2+} and IP_3 receptor-dependent release of Ca^{2+} stored in the endoplasmic reticulum, which could reactivate iNOS, COX_2, EP_1 metabotropic receptors and Cx43 hemichannels (not depicted). Meanwhile, the opening of Cx43 hemichannels contributes to the reduction of the insulin-mediated uptake and intercellular diffusion of glucose caused by IFN-γ plus high glucose. Alongside this, the uncontrolled activation of Cx43 hemichannels also increases the production of superoxide anion by the mitochondria and also reduces cell survival.

directly in the release of ATP from endothelial cells, given that they are permeable to this biomolecule [72]. In parallel, because Cx43 hemichannels are conduits for Ca^{2+} [76], they indirectly may cooperate to preserve $[Ca^{2+}]_i$-dependent signaling linked to ATP release. In line with that, IFN-γ plus high glucose caused a notable increase in ATP-induced Ca^{2+} responses compared to control conditions, specially, with regard to peak amplitude, integrated area and sustained signal. Remarkably, inhibition of Cx43 hemichannels completely blunted the enhanced responses in Ca^{2+} dynamics evoked by IFN-γ and high glucose. This evidence denotes that activation of Cx43 hemichannels are fundamental for the increased responses in ATP-mediated Ca^{2+} dynamics evoked by IFN-γ plus high glucose but not for the changes in basal Ca^{2+} levels.

Recently, we reported that high glucose and IL-1β/TNF-α enhances both basal and insulin-induced production of NO in endothelial cells [13]. In contrast with this data, we noted that IFN-γ plus high glucose increased basal levels of NO, but impede the normal rise of NO production evoked by insulin in endothelial cells. These findings harmonize with studies describing that insulin-mediated NO production and is impaired in endothelial cells subjected to inflammatory mediators [77,78]. In addition, we found that although IFN-γ plus high glucose did not alter basal glucose uptake in EAhy cells, they caused a dramatic reduction in glucose uptake evoked by insulin. Insulin is a well-known direct-acting vasodilator of the vasculature [79] and underpins glucose uptake by peripheral tissues [80] through mechanisms that may require the close coordination of endothelial cells via gap junctional communication [81]. Interestingly, we observed that IFN-γ plus high glucose strongly reduced the basal and insulin-dependent rise in intercellular diffusion of glucose mediated by gap junctions. The latter agrees with the fact that IFN-γ plus high glucose abrogated the gap junctional diffusion of LY likely via the endocytosis and degradation of Cx43 gap junctions. Of note, both gap19 and Tat-L2 greatly prevented the IFN-γ and high glucose-induced loss of response to insulin in terms of glucose uptake and intercellular diffusion, suggesting that activation of Cx43 hemichannels are crucial for those processes.

High Cx43 hemichannel activity reduces the chemical gradient across the cell membrane, which causes important drop in cell membrane potential [82]. Part of this consequence on membrane depolarization can be explained by the permeability of Cx43 hemichannels to Ca^{2+} [76] and the strongest driving force for Ca^{2+} influx imposed by its

great concentration difference between the extra and intra cellular space. The above can also account for the significant increase in cytosolic Ca^{2+} signal induced by ATP in endothelial cells treated with IFN-γ plus high glucose. Moreover, the increase in intracellular Ca^{2+} signal is likely to contribute to a mitochondria dysfunction. In fact, under pathological conditions, Ca^{2+} overload participates in the generation of ROS in mitochondria, followed by opening of the transient permeability pore (PPT) and cell death [83]. Furthermore, Ca^{2+} induces a decrease in the pH of the medium, stimulates respiration, generates a cycle of swelling and contraction of the mitochondria, oxidizes NADH and increases the redox state of the respiratory chain [84,85]. In this line, we found that IFN-γ or high glucose dramatically incremented the production of superoxide anion by mitochondria, which likely was implicated in the decreased cell survival observed under these conditions. More relevant to this point, these responses were strongly prevented by the blockade of Cx43 hemichannels. Bringing to light that endothelial Cx43 hemichannels significantly contribute to endothelial cell dysfunction and death, which could play a critical role in the pathogenesis of vascular diseases linked to insulin resistance. In addition, these findings might have relevant for the developing of atherosclerosis secondary to diabetes since IFN-γ and high glucose are well recognized pro-inflammatory agents worsen these pathological conditions [5Chait, 2009 #290, 8, 9].

In agreement with the involvement of Cx43 hemichannels in endothelial dysfunction, the IFN-γ and high glucose-induced alterations in ATP release, cytoplasmic Ca^{2+}, and insulin-mediated NO production, along with the alterations on the uptake and intercellular diffusion of glucose, were prominently abrogated by the inhibition of endothelial Cx43 hemichannels. These data are consistent with previous evidence indicating that inhibition of connexin hemichannels prevents renal damage observed in diabetic rats [86]. In addition, here, we showed the involvement of a series of molecular pathways and cellular processes that culminated in the opening of Cx43 hemichannels, such as the activation of P38 MAPK/COX_2/EP_1/PLC/IP_3 cascades, production of IL-1β/TNF-α, NO, PGE_2 and ATP, in addition to increased cytoplasmic Ca^{2+} dynamics (Fig. 11). We speculate that overall this machinery may embrace a self-perpetuating process, where both NO (likely via S-nitrosylation) or raise in $[Ca^{2+}]_i$ may reactivate Cx43 hemichannels with potential significant consequences for the function, inflammatory profile and survival of endothelial cells (Fig. 11). In agreement with this notion, we observed that EAhy cells treated with IFN-γ plus high glucose displayed a prominent production of mitochondrial superoxide anion and decreased cell survival upon several days of treatment, the latter being a response completely blunted by inhibition of Cx43 hemichannels.

We propose that mitigating Cx43 hemichannel activity through selective blockers at the endothelium might constitute a new approach against the activation of pernicious pathways that cause endothelial dysfunction and resistance to insulin signaling and possibly cell damage evoked by pro-inflammatory cytokines and high glucose.

CRediT authorship contribution statement

Juan C. Sáez:Conceptualization, Data curation, Writing - review & editing.**Susana Contreras-Duarte**:Conceptualization, Data curation, Formal analysis, Investigation, Methodology, Validation, Writing - review & editing.**Valeria C. Labra**:Investigation, Methodology, Project administration, Resources, Software, Supervision, Validation.**Cristian A. Santibañez**:Investigation, Methodology, Project administration, Resources, Software, Supervision, Validation.**Luis A. Mellado**:Methodology, Resources, Project administration.**Carla A. Inostroza**:Methodology, Resources, Project administration.**Tanhia F. Alvear**:Methodology, Resources, Project administration.**Mauricio A. Retamal**:Data curation, Formal analysis, Investigation, Writing - review & editing.**Victoria Velarde**:Conceptualization, Writing - review & editing.**Juan A. Orellana**:Conceptualization, Data curation, Formal analysis, Funding acquisition, Investigation, Methodology, Software, Supervision, Validation, Visualization, Writing - original draft, Writing - review & editing.

Declaration of competing interest

The authors declare that they have no known competing financial interests or personal relationships that could have appeared to influence the work reported in this paper.

Acknowledgments

This work was supported by the Fondo Nacional de Desarrollo Científico y Tecnológico (FONDECYT) Grant 1160710 (to JAO), 1191329 (to JCS), the Comisión Nacional de Investigación Científica y Tecnológica (CONICYT) and Programa de Investigación Asociativa (PIA) Grant Anillo de Ciencia y Tecnología ACT1411 (to JAO), P09-022-F from ICM-ECONOMIA, Chile (to JCS).

References

[1] C.M. Boulanger, Highlight on endothelial activation and beyond, Arterioscler. Thromb. Vasc. Biol. 38 (2018) e198–e201.
[2] J.S. Pober, W.C. Sessa, Inflammation and the blood microvascular system, Cold Spring Harb. Perspect. Biol. 7 (2014) a016345.
[3] K. Pyorala, M. Laakso, M. Uusitupa, Diabetes and atherosclerosis: an epidemiologic view, Diabetes Metab. Rev. 3 (1987) 463–524.
[4] T. Yuan, T. Yang, H. Chen, D. Fu, Y. Hu, J. Wang, Q. Yuan, H. Yu, W. Xu, X. Xie, New insights into oxidative stress and inflammation during diabetes mellitus-accelerated atherosclerosis, Redox Biol. 20 (2019) 247–260.
[5] K.E. Bornfeldt, I. Tabas, Insulin resistance, hyperglycemia, and atherosclerosis, Cell Metab. 14 (2011) 575–585.
[6] A. Chait, K.E. Bornfeldt, Diabetes and atherosclerosis: is there a role for hyperglycemia? J. Lipid Res. 50 (Suppl) (2009) S335–S339.
[7] M.A. Gimbrone Jr., G. Garcia-Cardena, Endothelial cell dysfunction and the pathobiology of atherosclerosis, Circ. Res. 118 (2016) 620–636.
[8] X. Weng, X. Cheng, X. Wu, H. Xu, M. Fang, Y. Xu, Sin3B mediates collagen type I gene repression by interferon gamma in vascular smooth muscle cells, Biochem. Biophys. Res. Commun. 447 (2014) 263–270.
[9] J.E. McLaren, D.P. Ramji, Interferon gamma: a master regulator of atherosclerosis, Cytokine Growth Factor Rev. 20 (2009) 125–135.
[10] I. Voloshyna, M.J. Littlefield, A.B. Reiss, Atherosclerosis and interferon-gamma: new insights and therapeutic targets, Trends Cardiovasc Med 24 (2014) 45–51.
[11] A.H. Stolpen, E.C. Guinan, W. Fiers, J.S. Pober, Recombinant tumor necrosis factor and immune interferon act singly and in combination to reorganize human vascular endothelial cell monolayers, Am. J. Pathol. 123 (1986) 16–24.
[12] C.T. Ng, L.Y. Fong, M.R. Sulaiman, M.A. Moklas, Y.K. Yong, M.N. Hakim, Z. Ahmad, Interferon-gamma increases endothelial permeability by causing activation of p38 MAP kinase and actin cytoskeleton alteration, J. Interf. Cytokine Res. 35 (2015) 513–522.
[13] J.C. Saez, S. Contreras-Duarte, G.I. Gomez, V.C. Labra, C.A. Santibanez, R. Gajardo-Gomez, B.C. Avendano, E.F. Diaz, T.D. Montero, V. Velarde, J.A. Orellana, Connexin 43 Hemichannel activity promoted by pro-inflammatory cytokines and high glucose alters endothelial cell function, Front. Immunol. 9 (2018) 1899.
[14] M.A. Retamal, E.P. Reyes, I.E. Garcia, B. Pinto, A.D. Martinez, C. Gonzalez, Diseases associated with leaky hemichannels, Front. Cell. Neurosci. 9 (2015) 267.
[15] J.C. Saez, L. Leybaert, Hunting for connexin hemichannels, FEBS Lett. 588 (2014) 1205–1211.
[16] L. Leybaert, P.D. Lampe, S. Dhein, B.R. Kwak, P. Ferdinandy, E.C. Beyer, D.W. Laird, C.C. Naus, C.R. Green, R. Schulz, Connexins in cardiovascular and neurovascular health and disease: pharmacological implications, Pharmacol. Rev. 69 (2017) 396–478.
[17] Y. Kim, J.O. Davidson, K.C. Gunn, A.R. Phillips, C.R. Green, A.J. Gunn, Role of Hemichannels in CNS inflammation and the Inflammasome pathway, Advances in protein chemistry and structural biology 104 (2016) 1–37.
[18] P.J. Saez, K.F. Shoji, M.A. Retamal, P.A. Harcha, G. Ramirez, J.X. Jiang, R. von Bernhardi, J.C. Saez, ATP is Required and Advances Cytokine-induced Gap Junction Formation in Microglia In Vitro, Mediat Inflamm (2013).
[19] R.G. Johnson, H.C. Le, K. Evenson, S.W. Loberg, T.M. Myslajek, A. Prabhu, A.M. Manley, C. O'Shea, H. Grunenwald, M. Haddican, P.M. Fitzgerald, T. Robinson, B.A. Cisterna, J.C. Saez, T.F. Liu, D.W. Laird, J.D. Sheridan, Connexin Hemichannels: methods for dye uptake and leakage, J. Membr. Biol. 249 (2016) 713–741.
[20] R. Ponsaerts, E. De Vuyst, M. Retamal, C. D'Hondt, D. Vermeire, N. Wang, H. De Smedt, P. Zimmermann, B. Himpens, J. Vereecke, L. Leybaert, G. Bultynck, Intramolecular loop/tail interactions are essential for connexin 43-hemichannel activity, FASEB journal : official publication of the Federation of American Societies for Experimental Biology 24 (2010) 4378–4395.

[21] N. Wang, M. De Bock, E. Decrock, M. Bola, A. Gadicherla, G. Bultynck, L. Leybaert, Connexin targeting peptides as inhibitors of voltage- and intracellular Ca2+ −triggered Cx43 hemichannel opening, Neuropharmacology 75 (2013) 506–516.

[22] N. Wang, M. De Bock, G. Antoons, A.K. Gadicherla, M. Bol, E. Decrock, W.H. Evans, K.R. Sipido, F.F. Bukauskas, L. Leybaert, Connexin mimetic peptides inhibit Cx43 hemichannel opening triggered by voltage and intracellular Ca2+ elevation, Basic Res. Cardiol. 107 (2012) 304.

[23] C. D'Hondt, R. Ponsaerts, H. De Smedt, G. Bultynck, B. Himpens, Pannexins, distant relatives of the connexin family with specific cellular functions? Bioessays 31 (2009) 953–974.

[24] S. Godecke, C. Roderigo, C.R. Rose, B.H. Rauch, A. Godecke, J. Schrader, Thrombin-induced ATP release from human umbilical vein endothelial cells, American journal of physiology. Cell physiology 302 (2012) C915–C923.

[25] Y. Kaneko, M. Tachikawa, R. Akaogi, K. Fujimoto, M. Ishibashi, Y. Uchida, P.O. Couraud, S. Ohtsuki, K. Hosoya, T. Terasaki, Contribution of pannexin 1 and connexin 43 hemichannels to extracellular calcium-dependent transport dynamics in human blood-brain barrier endothelial cells, J. Pharmacol. Exp. Ther. 353 (2015) 192–200.

[26] A.W. Lohman, I.L. Leskov, J.T. Butcher, S.R. Johnstone, T.A. Stokes, D. Begandt, L.J. DeLalio, A.K. Best, S. Penuela, N. Leitinger, K.S. Ravichandran, K.Y. Stokes, B.E. Isakson, Pannexin 1 channels regulate leukocyte emigration through the venous endothelium during acute inflammation, Nat. Commun. 6 (2015) 7965.

[27] P.S. Gaete, M.A. Lillo, M. Puebla, I. Poblete, X.F. Figueroa, CGRP signalling inhibits NO production through pannexin-1 channel activation in endothelial cells, Sci. Rep. 9 (2019) 7932.

[28] M.A. Retamal, C.J. Cortes, L. Reuss, M.V. Bennett, J.C. Saez, S-nitrosylation and permeation through connexin 43 hemichannels in astrocytes: induction by oxidant stress and reversal by reducing agents, Proc. Natl. Acad. Sci. U. S. A. 103 (2006) 4475–4480.

[29] B.C. Avendano, T.D. Montero, C.E. Chavez, R. von Bernhardi, J.A. Orellana, Prenatal exposure to inflammatory conditions increases Cx43 and Panx1 unopposed channel opening and activation of astrocytes in the offspring effect on neuronal survival, Glia 63 (2015) 2058–2072.

[30] M.A. Retamal, N. Froger, N. Palacios-Prado, P. Ezan, P.J. Saez, J.C. Saez, C. Giaume, Cx43 hemichannels and gap junction channels in astrocytes are regulated oppositely by proinflammatory cytokines released from activated microglia, J. Neurosci. 27 (2007) 13781–13792.

[31] Z.F. Liu, D. Zheng, G.C. Fan, T. Peng, L. Su, Heat stress prevents lipopolysaccharide-induced apoptosis in pulmonary microvascular endothelial cells by blocking calpain/p38 MAPK signalling, Apoptosis : an international journal on programmed cell death 21 (2016) 896–904.

[32] W. Pan, H. Yu, S. Huang, P. Zhu, Resveratrol protects against TNF-alpha-induced injury in human umbilical endothelial cells through promoting Sirtuin-1-induced repression of NF-KB and p38 MAPK, PLoS One 11 (2016) e0147034.

[33] D. Salvemini, T.P. Misko, J.L. Masferrer, K. Seibert, M.G. Currie, P. Needleman, Nitric oxide activates cyclooxygenase enzymes, Proc. Natl. Acad. Sci. U. S. A. 90 (1993) 7240–7244.

[34] S. Park, B. Sung, E.J. Jang, D.H. Kim, C.H. Park, Y.J. Choi, Y.M. Ha, M.K. Kim, N.D. Kim, B.P. Yu, H.Y. Chung, Inhibitory action of salicylideneamino-2-thiophenol on NF-kappaB signaling cascade and cyclooxygenase-2 in HNE-treated endothelial cells, Arch. Pharm. Res. 36 (2013) 880–889.

[35] E.F. Diaz, V.C. Labra, T.F. Alvear, L.A. Mellado, C.A. Inostroza, J.E. Oyarzun, N. Salgado, R.A. Quintanilla, J.A. Orellana, Connexin 43 hemichannels and pannexin-1 channels contribute to the alpha-synuclein-induced dysfunction and death of astrocytes, Glia 67 (2019) 1598–1619.

[36] J.A. Orellana, T.D. Montero, R. von Bernhardi, Astrocytes inhibit nitric oxide-dependent Ca(2+) dynamics in activated microglia: involvement of ATP released via pannexin 1 channels, Glia 61 (2013) 2023–2037.

[37] A. Lissoni, P. Hulpiau, T. Martins-Marques, N. Wang, G. Bultynck, R. Schulz, K. Witschas, H. Girao, M. De Smet, L. Leybaert, RyR2 regulates Cx43 hemichannel intracellular Ca2+ −dependent activation in cardiomyocytes, Cardiovasc. Res. (2019), https://doi.org/10.1093/cvr/cvz340 (Epub ahead of print).

[38] A. Alvarez, R. Lagos-Cabre, M. Kong, A. Cardenas, F. Burgos-Bravo, P. Schneider, A.F. Quest, L. Leyton, Integrin-mediated transactivation of P2X7R via hemichannel-dependent ATP release stimulates astrocyte migration, Biochim. Biophys. Acta 1863 (2016) 2175–2188.

[39] A. Baroja-Mazo, M. Barbera-Cremades, P. Pelegrin, The participation of plasma membrane hemichannels to purinergic signaling, Biochim. Biophys. Acta 1828 (2013) 79–93.

[40] J.A. Orellana, P.J. Saez, K.F. Shoji, K.A. Schalper, N. Palacios-Prado, V. Velarde, C. Giaume, M.V. Bennett, J.C. Saez, Modulation of brain hemichannels and gap junction channels by pro-inflammatory agents and their possible role in neurodegeneration, Antioxid. Redox Signal. 11 (2009) 369–399.

[41] J. Willebrords, S. Crespo Yanguas, M. Maes, E. Decrock, N. Wang, L. Leybaert, B.R. Kwak, C.R. Green, B. Cogliati, M. Vinken, Connexins and their channels in inflammation, Crit. Rev. Biochem. Mol. Biol. 51 (2016) 413–439.

[42] J.C. Saez, V.M. Berthoud, M.C. Branes, A.D. Martinez, E.C. Beyer, Plasma membrane channels formed by connexins: their regulation and functions, Physiol. Rev. 83 (2003) 1359–1400.

[43] M. Lind, A. Hayes, M. Caprnda, D. Petrovic, L. Rodrigo, P. Kruzliak, A. Zulli, Inducible nitric oxide synthase: good or bad? Biomedicine & pharmacotherapy = Biomedecine & pharmacotherapie 93 (2017) 370–375.

[44] M. Dosch, J. Gerber, F. Jebbawi, G. Beldi, Mechanisms of ATP release by inflammatory cells, Int J Mol Sci 19 (2018).

[45] Y. Kim, J.M. Griffin, P.W.R. Harris, S.H.C. Chan, L.F.B. Nicholson, M.A. Brimble, S.J. O'Carroll, C.R. Green, Characterizing the mode of action of extracellular Connexin43 channel blocking mimetic peptides in an in vitro ischemia injury model, Bba-Gen Subjects 1861 (2017) 68–78.

[46] J. Robertson, S. Lang, P.A. Lambert, P.E. Martin, Peptidoglycan derived from Staphylococcus epidermidis induces Connexin43 hemichannel activity with consequences on the innate immune response in endothelial cells, The Biochemical journal 432 (2010) 133–143.

[47] D.F. Woodward, R.L. Jones, S. Narumiya, International Union of Basic and Clinical Pharmacology. LXXXIII: classification of prostanoid receptors, updating 15 years of progress, Pharmacological reviews, 63 (2011) 471–538.

[48] M. De Bock, N. Wang, M. Bol, E. Decrock, R. Ponsaerts, G. Bultynck, G. Dupont, L. Leybaert, Connexin 43 hemichannels contribute to cytoplasmic Ca2+ oscillations by providing a bimodal Ca2+ −dependent Ca2+ entry pathway, J. Biol. Chem. 287 (2012) 12250–12266.

[49] W. Li, X. Yang, T. Zheng, S. Xing, Y. Wu, F. Bian, G. Wu, Y. Li, J. Li, X. Bai, D. Wu, X. Jia, L. Wang, L. Zhu, S. Jin, TNF-alpha stimulates endothelial palmitic acid transcytosis and promotes insulin resistance, Sci. Rep. 7 (2017) 44659.

[50] Y. Zhang, T. Liu, Y. Chen, Z. Dong, J. Zhang, Y. Sun, B. Jin, F. Gao, S. Guo, R. Zhuang, CD226 reduces endothelial cell glucose uptake under hyperglycemic conditions with inflammation in type 2 diabetes mellitus, Oncotarget 7 (2016) 12010–12023.

[51] A. Janus, E. Szahidewicz-Krupska, G. Mazur, A. Doroszko, Insulin resistance and endothelial dysfunction constitute a common therapeutic target in Cardiometabolic disorders, Mediat. Inflamm. 2016 (2016) 3634948.

[52] J. Niu, T. Li, C. Yi, N. Huang, A. Koulakoff, C. Weng, C. Li, C.J. Zhao, C. Giaume, L. Xiao, Connexin-based channels contribute to metabolic pathways in the oligodendroglial lineage, J. Cell Sci. 129 (2016) 1902–1914.

[53] Q. Chang, W. Tang, S. Ahmad, B. Zhou, X. Lin, Gap junction mediated intercellular metabolite transfer in the cochlea is compromised in connexin30 null mice, PLoS One 3 (2008) e4088.

[54] T. Suzuki, T. Matsunami, Y. Hisa, K. Takata, T. Takamatsu, M. Oyamada, Roles of gap junctions in glucose transport from glucose transporter 1-positive to -negative cells in the lateral wall of the rat cochlea, Histochem. Cell Biol. 131 (2009) 89–102.

[55] G.K. Gandhi, N.F. Cruz, K.K. Ball, S.A. Theus, G.A. Dienel, Selective astrocytic gap junctional trafficking of molecules involved in the glycolytic pathway: impact on cellular brain imaging, J. Neurochem. 110 (2009) 857–869.

[56] H. Liu, H. Xiang, S. Zhao, H. Sang, F. Lv, R. Chen, Z. Shu, A.F. Chen, S. Chen, H. Lu, Vildagliptin improves high glucose-induced endothelial mitochondrial dysfunction via inhibiting mitochondrial fission, J. Cell. Mol. Med. 23 (2019) 798–810.

[57] L. Piconi, L. Quagliaro, R. Assaloni, R. Da Ros, A. Maier, G. Zuodar, A. Ceriello, Constant and intermittent high glucose enhances endothelial cell apoptosis through mitochondrial superoxide overproduction, Diabetes Metab. Res. Rev. 22 (2006) 198–203.

[58] J.H. Li, J.S. Pober, The cathepsin B death pathway contributes to TNF plus IFN-gamma-mediated human endothelial injury, J. Immunol. 175 (2005) 1858–1866.

[59] Y. Chi, X. Zhang, Z. Zhang, T. Mitsui, M. Kamiyama, M. Takeda, J. Yao, Connexin43 hemichannels contributes to the disassembly of cell junctions through modulation of intracellular oxidative status, Redox Biol. 9 (2016) 198–209.

[60] Z. Zhang, S. Zhang, Y. Wang, M. Yang, N. Zhang, Z. Jin, L. Ding, W. Jiang, J. Yang, Z. Sun, C. Qiu, T. Hu, Autophagy inhibits high glucose induced cardiac microvascular endothelial cells apoptosis by mTOR signal pathway, Apoptosis : an international journal on programmed cell death 22 (2017) 1510–1523.

[61] S.H. Javanmard, N. Dana, The effect of interferon gamma on endothelial cell nitric oxide production and apoptosis, Adv Biomed Res 1 (2012) 69.

[62] N. Koide, A. Morikawa, G. Tumurkhuu, J. Dagvadorj, F. Hassan, S. Islam, Y. Naiki, I. Mori, T. Yoshida, T. Yokochi, Lipopolysaccharide and interferon-gamma enhance Fas-mediated cell death in mouse vascular endothelial cells via augmentation of Fas expression, Clin. Exp. Immunol. 150 (2007) 553–560.

[63] C.E. Chavez, J.E. Oyarzun, B.C. Avendano, L.A. Mellado, C.A. Inostroza, T.F. Alvear, J.A. Orellana, The opening of connexin 43 hemichannels alters hippocampal astrocyte function and neuronal survival in prenatally LPS-exposed adult offspring, Front. Cell. Neurosci. 13 (2019) 460.

[64] A.K. Gadicherla, N. Wang, M. Bulic, E. Agullo-Pascual, A. Lissoni, M. De Smet, M. Delmar, G. Bultynck, D.V. Krysko, A. Camara, K.D. Schluter, R. Schulz, W.M. Kwok, L. Leybaert, Mitochondrial Cx43 hemichannels contribute to mitochondrial calcium entry and cell death in the heart, Basic Res. Cardiol. 112 (2017) 27.

[65] D.R. Wesemann, E.N. Benveniste, STAT-1 alpha and IFN-gamma as modulators of TNF-alpha signaling in macrophages: regulation and functional implications of the TNF receptor 1:STAT-1 alpha complex, J. Immunol. 171 (2003) 5313–5319.

[66] K. Ohta, T. Naruse, H. Kato, Y. Ishida, T. Nakagawa, S. Ono, H. Shigeishi, M. Takechi, Differential regulation by IFNgamma on TNFalphainduced chemokine expression in synovial fibroblasts from temporomandibular joint, Mol. Med. Rep. 16 (2017) 6850–6857.

[67] L. Tolosa, M. Morla, A. Iglesias, X. Busquets, J. Llado, G. Olmos, IFN-gamma prevents TNF-alpha-induced apoptosis in C2C12 myotubes through down-regulation of TNF-R2 and increased NF-kappaB activity, Cell. Signal. 17 (2005) 1333–1342.

[68] J.L. Stahl, E.B. Cook, F.M. Graziano, N.P. Barney, Differential and cooperative effects of TNFalpha, IL-1beta, and IFNgamma on human conjunctival epithelial cell receptor expression and chemokine release, Invest. Ophthalmol. Vis. Sci. 44 (2003) 2010–2015.

[69] T. Eigenbrod, K.A. Bode, A.H. Dalpke, Early inhibition of IL-1beta expression by IFN-gamma is mediated by impaired binding of NF-kappaB to the IL-1beta promoter but is independent of nitric oxide, J. Immunol. 190 (2013) 6533–6541.

[70] T.A. Swierkosz, J.A. Mitchell, T.D. Warner, R.M. Botting, J.R. Vane, Co-induction of nitric oxide synthase and cyclo-oxygenase: interactions between nitric oxide and

prostanoids, Br. J. Pharmacol. 114 (1995) 1335–1342.
[71] V. Abudara, M.A. Retamal, R. Del Rio, J.A. Orellana, Synaptic functions of Hemichannels and Pannexons: a double-edged sword, Front. Mol. Neurosci. 11 (2018) 435.
[72] J. Kang, N. Kang, D. Lovatt, A. Torres, Z. Zhao, J. Lin, M. Nedergaard, Connexin 43 hemichannels are permeable to ATP, J. Neurosci. 28 (2008) 4702–4711.
[73] J.A. Orellana, D. Busso, G. Ramirez, M. Campos, A. Rigotti, J. Eugenin, R. von Bernhardi, Prenatal nicotine exposure enhances Cx43 and Panx1 unopposed channel activity in brain cells of adult offspring mice fed a high-fat/cholesterol diet, Front. Cell. Neurosci. 8 (2014) 403.
[74] J.A. Orellana, P.J. Saez, C. Cortes-Campos, R.J. Elizondo, K.F. Shoji, S. Contreras-Duarte, V. Figueroa, V. Velarde, J.X. Jiang, F. Nualart, J.C. Saez, M.A. Garcia, Glucose increases intracellular free Ca(2+) in tanycytes via ATP released through connexin 43 hemichannels, Glia 60 (2012) 53–68.
[75] C. Meunier, N. Wang, C. Yi, G. Dallerac, P. Ezan, A. Koulakoff, L. Leybaert, C. Giaume, Contribution of Astroglial Cx43 Hemichannels to the modulation of Glutamatergic currents by D-serine in the mouse prefrontal cortex, J. Neurosci. 37 (2017) 9064–9075.
[76] K.A. Schalper, H.A. Sanchez, S.C. Lee, G.A. Altenberg, M.H. Nathanson, J.C. Saez, Connexin 43 hemichannels mediate the Ca2+ influx induced by extracellular alkalinization, American journal of physiology. Cell physiology 299 (2010) C1504–C1515.
[77] F. Andreozzi, E. Laratta, C. Procopio, M.L. Hribal, A. Sciacqua, M. Perticone, C. Miele, F. Perticone, G. Sesti, Interleukin-6 impairs the insulin signaling pathway, promoting production of nitric oxide in human umbilical vein endothelial cells, Mol. Cell. Biol. 27 (2007) 2372–2383.
[78] I.P. Salt, V.A. Morrow, F.M. Brandie, J.M. Connell, J.R. Petrie, High glucose inhibits insulin-stimulated nitric oxide production without reducing endothelial nitric-oxide synthase Ser1177 phosphorylation in human aortic endothelial cells, J. Biol. Chem. 278 (2003) 18791–18797.
[79] U. Scherrer, D. Randin, P. Vollenweider, L. Vollenweider, P. Nicod, Nitric oxide release accounts for insulin's vascular effects in humans, J. Clin. Invest. 94 (1994) 2511–2515.
[80] S.J. Cleland, J.R. Petrie, S. Ueda, H.L. Elliott, J.M. Connell, Insulin-mediated vasodilation and glucose uptake are functionally linked in humans, Hypertension 33 (1999) 554–558.
[81] X.F. Figueroa, B.R. Duling, Gap junctions in the control of vascular function, Antioxid. Redox Signal. 11 (2009) 251–266.
[82] A.A. Vargas, B.A. Cisterna, F. Saavedra-Leiva, C. Urrutia, L.A. Cea, A.H. Vielma, S.E. Gutierrez-Maldonado, A.J. Martin, C. Pareja-Barrueto, Y. Escalona, O. Schmachtenberg, C.F. Lagos, T. Perez-Acle, J.C. Saez, On biophysical properties and sensitivity to gap junction blockers of Connexin 39 Hemichannels expressed in HeLa cells, Front. Physiol. 8 (2017) 38.
[83] P.S. Brookes, Y. Yoon, J.L. Robotham, M.W. Anders, S.S. Sheu, Calcium, ATP, and ROS: a mitochondrial love-hate triangle, American journal of physiology. Cell physiology 287 (2004) C817–C833.
[84] B. O'Rourke, Mitochondrial ion channels, Annu. Rev. Physiol. 69 (2007) 19–49.
[85] P.M. Peixoto, S.Y. Ryu, K.W. Kinnally, Mitochondrial ion channels as therapeutic targets, FEBS Lett. 584 (2010) 2142–2152.
[86] R. Hernandez-Salinas, A.Z. Vielma, M.N. Arismendi, M.P. Boric, J.C. Saez, V. Velarde, Boldine prevents renal alterations in diabetic rats, J. Diabetes Res. 2013 (2013) 593672.